






One-Bit Spectrum Sensing for Cognitive Radio

Pei-Wen Wu , Lei Huang , *Senior Member, IEEE*, David Ramírez , *Senior Member, IEEE*, Yu-Hang Xiao , *Member, IEEE*, and Hing Cheung So , *Fellow, IEEE*

Abstract—Spectrum sensing for cognitive radio requires effective monitoring of wide bandwidths, which translates into high-rate sampling. Traditional spectrum sensing methods employing high-precision analog-to-digital converters (ADCs) result in increased power consumption and expensive hardware costs. In this paper, we explore blind spectrum sensing utilizing one-bit ADCs. We derive a closed-form detector based on Rao’s test and demonstrate its equivalence with the second-order eigenvalue-moment-ratio test. Furthermore, a near-exact distribution based on the moment-based method, and an approximate distribution in the low signal-to-noise ratio (SNR) regime based on the central limit theorem, are obtained. Theoretical analysis is then performed and our results show that the performance loss of the proposed detector is approximately 2 dB ($\pi/2$) compared to detectors employing ∞ -bit ADCs when the SNR is low. This loss can be compensated for by using approximately 2.47 ($\pi^2/4$) times more samples. In addition, we unveil that the efficiency of incoherent accumulation in one-bit detection is the square root of that of coherent accumulation. Simulation results corroborate the correctness of our theoretical calculations.

Index Terms—One-bit ADC, performance degradation, Rao’s test, spectrum sensing.

I. INTRODUCTION

SPECTRUM sensing is a crucial prerequisite for the dynamic allocation of spectrum resources in cognitive radio (CR) networks, as it is responsible for finding vacant channels

Manuscript received 23 June 2023; revised 30 October 2023; accepted 6 December 2023. Date of publication 4 January 2024; date of current version 15 January 2024. The work of Lei Huang was supported in part by the National Science Fund for Distinguished Young Scholars under Grant 61925108, in part by the Key Project of International Cooperation and Exchanges of the National Natural Science Foundation of China under Grant 62220106009, in part by the project of Shenzhen Peacock Plan Teams under Grant KQTD20210811090051046, and in part by the Shenzhen University 2035 Program for Excellent Research. The work of David Ramírez was supported in part by MCIN/AEI/10.13039/501100011033/FEDER, UE, under Grant PID2021-123182OB-I00 (EPICENTER), and in part by the Office of Naval Research (ONR) Global under Contract N62909-23-1-2002. The work of Yu-Hang Xiao was supported by the National Natural Science Foundation of China under Grant 62201359. The associate editor coordinating the review of this manuscript and approving it for publication was Prof. Pascal Vallet. (Corresponding authors: Lei Huang; Yu-Hang Xiao.)

Pei-Wen Wu, Lei Huang, and Yu-Hang Xiao are with the State Key Laboratory of Radio Frequency Heterogeneous Integration (Shenzhen University), Shenzhen University, Shenzhen 518060, China (e-mail: wupeiwu2021@szu.edu.cn; dr.lei.huang@ieee.org; yuhangxiao@szu.edu.cn).

David Ramírez is with the Department of Signal Theory and Communications, Universidad Carlos III de Madrid, Madrid 28903, Spain, and also with Gregorio Marañón Health Research Institute, Madrid 28007, Spain (e-mail: david.ramirez@uc3m.es).

Hing Cheung So is with the Department of Electrical Engineering, City University of Hong Kong, Hong Kong 999077, China (e-mail: hcso@ee.cityu.edu.hk).

Digital Object Identifier 10.1109/TSP.2023.3343569

(a.k.a. spectrum holes) [1], [2], [3], [4], [5]. In many application scenarios, the task is to monitor wideband channels, which translates into high-speed sampling. However, traditional spectrum sensing methods typically require high-precision quantization to achieve optimal performance. Such high-speed and high-precision sampling results in large energy consumption, which may not be practically feasible.

To address this problem, an effective method is to decrease the quantization accuracy, particularly by using only one-bit analog-to-digital converters (ADCs) [6]. One-bit ADCs only require a single comparator to complete the sampling and quantization process, offering advantages such as high sampling rate, low hardware complexity, and low power consumption compared to high-precision sampling [7], [8], [9]. For example, at a sampling rate of 3.2 GSPS/s, an 8-bit ADC sampling [10] requires 105 mWatts while the one-bit ADC sampling [11] consumes only 20 μ Watts. Furthermore, the performance loss of one-bit radar detectors proposed in [12] is only 2 dB ($\pi/2$) at low signal-to-noise ratios (SNRs), which can be compensated via increasing the number of samples by a factor $\pi/2$. These merits motivate the application of one-bit sampling techniques to spectrum sensing.

Many one-bit detection problems assume the availability of prior information, such as noise power, channel parameter characteristics, and/or signal characteristics [9], [12], [13], [14], [15]. However, this work focuses on one-bit spectrum sensing in the absence of prior information, also known as blind spectrum sensing. In this case, the probability mass function (PMF) of the one-bit observations is the product of orthonormal probabilities, which does not have a closed-form expression [16], [17], [18]. Therefore, numerical techniques are needed when designing detectors using standard methods, e.g., generalized likelihood ratio test (GLRT) [19]. In addition, numerical methods result in higher computational time and costs, contradicting the original purpose for simple spectrum sensing [20]. Therefore, a closed-form detector is desirable.

A closed-form one-bit eigenvalue moment ratio (EMR) detector, inspired by the EMR detector [21], was proposed in [22]. It was demonstrated that the one-bit EMR is 3 dB inferior to the ∞ -bit EMR. However, performance degradation of one-bit sampling was proven to be only 2 dB when the SNR is low [23]. The result has been further corroborated in one-bit detection by [12], [19], and other one-bit signal processing problems by [24], [25], [26], [27], [28], [29]. The increased performance loss is due to the fact that the one-bit EMR is obtained by initially stacking the real and imaginary parts of the one-bit complex observations, followed by computing the EMR

of the corresponding real-valued covariance matrix, neglecting the circularity property of the unquantized signals.

In this paper, we formulate a detector for one-bit observations following the rule of Rao's test and taking into account the circularity property to enhance performance. The result turns out to be the second-order EMR of the one-bit complex-valued sample covariance matrix, rather than the expanded real-valued covariance matrix as presented in [22].

To verify the 2 dB loss, we analyze the performance degradation by comparing the proposed one-bit Rao's test with its ∞ -bit counterpart. To enable such a comparison, we derive approximate distributions of the proposed detector under only noise and low SNRs, which yield results that can be compared to the asymptotic distribution derived in [30]. In particular, the null distribution follows the same χ^2 distribution, while the non-null distributions in the low SNRs are all non-central χ^2 distributions, albeit with different non-centrality parameters. By examining the non-centrality parameters, we can effectively quantify the performance degradation. In higher SNR scenarios, where the approximation breaks, a near-exact Beta-approximation using the moment-based method [3], [4], [5], [31] is also provided.

The contributions of this paper are as follows:

- 1) We present a novel detector based on Rao's test for blind spectrum sensing utilizing one-bit ADCs. The proposed detector is formulated in a closed-form manner, eliminating the need for numerical optimization. Moreover, we demonstrate that the proposed detector is equivalent to the second-order EMR detector (or John's detector [32], [33]) using complex-valued one-bit observations. Our detector outperforms the one-bit EMR detector [22], which adopts the expanded real-valued covariance matrix.
- 2) We derive near-exact null and non-null distributions of the proposed detector, enabling the calculation of false alarm and detection probabilities. Additionally, approximate null and non-null distributions under low SNRs are obtained, simplifying performance comparison.
- 3) We prove that the performance loss of the proposed detector in low SNR environments is approximately 2 dB ($\pi/2$) compared to the detector using ∞ -bit ADCs, which is smaller than the 3 dB performance loss reported in [22]. Moreover, this loss can be compensated for by increasing the number of samples of our detector by a factor of approximately 2.47 ($\pi^2/4$).
- 4) Upon comparison with the findings in [12], we arrive at an intriguing conclusion: The efficiency of coherent accumulation in one-bit detection is the square of that of non-coherent accumulation.

The structure of this paper is organized as follows. Section II presents the signal model for one-bit blind spectrum sensing. In Section III, a detector based on Rao's test is derived. The null and non-null distributions of the proposed detector are analyzed in Section IV. Section V examines the performance degradation when using one-bit ADCs in comparison to ∞ -bit ADCs. Simulation results are provided in Section VI to validate the theoretical calculations. Finally, Section VII offers a summary of the main conclusions.

Notation

Throughout this paper, we use boldface uppercase letters for matrices, boldface lowercase letters for column vectors, and light face lowercase letters for scalar quantities. The notation $\mathbf{A} \in \mathbb{R}^{p \times q}$ ($\mathbb{C}^{p \times q}$) indicates that \mathbf{A} is a $p \times q$ real (complex) matrix. The $\text{diag}(\mathbf{a})$ represents a diagonal matrix whose diagonal elements are the same as those of \mathbf{a} , while $\text{Diag}(\mathbf{A})$ represents a diagonal matrix whose diagonal elements are the same as those of the diagonal elements of \mathbf{A} . The operator $\|\cdot\|$ represents the Frobenius norm when its argument is a matrix, and the ℓ_2 norm when its argument is a vector. The trace of \mathbf{A} is $\text{tr}(\mathbf{A})$. The superscripts $(\cdot)^{-1}$, $(\cdot)^T$, and $(\cdot)^H$ represent matrix inverse, transpose, and Hermitian transpose operations. \mathbf{I}_a is the $a \times a$ identity matrix. The operator $\mathbb{E}[a]$ denotes the expected value and \sim means "distributed as." The central and non-central Chi-squared distributions are denoted by χ_k^2 and $\chi_k^2(\delta^2)$, respectively, where k is the number of degrees-of-freedom (DOFs) and δ^2 is the non-centrality parameter. Finally, the operators $\text{Re}(\cdot)$ and $\text{Im}(\cdot)$ extract the real and imaginary parts of their arguments, i is the imaginary unit, and $\text{sign}(\cdot)$ takes the sign of its argument.

II. SIGNAL MODEL

Consider a multiple-input multiple-output CR network where there are p single-antenna primary users (PUs) and m receiving antennas at the secondary user (SU). The input of the one-bit ADCs, $\mathbf{x}(t)$, $t = 1, \dots, n$, under \mathcal{H}_0 (signal absence) and \mathcal{H}_1 (signal presence) are given by [34], [35], [36]:

$$\begin{aligned} \mathcal{H}_0 : \mathbf{x}(t) &= \mathbf{w}(t), \\ \mathcal{H}_1 : \mathbf{x}(t) &= \mathbf{H}\mathbf{s}(t) + \mathbf{w}(t), \end{aligned} \quad (1)$$

where $\mathbf{H} \in \mathbb{C}^{m \times p}$ represents the unknown and deterministic channel coefficient during the sensing period. Here, $\mathbf{s}(t) = [s_1(t), \dots, s_p(t)]^T$ and $\mathbf{w}(t) = [w_1(t), \dots, w_m(t)]^T$ are the signal vector and the noise vector. In addition, the noise vector $\mathbf{w}(t) = [w_1(t), \dots, w_m(t)]^T$ follows i.i.d. zero mean circular symmetric complex Gaussian (ZMCSCG) distributions with unknown covariance matrix $\mathbf{R}_w = \text{diag}(\sigma_{w_1}, \dots, \sigma_{w_m})$, respectively. It is worth noting \mathbf{R}_w may have unequal diagonal elements, indicating the absence of calibration at the receiver [34], [37], [38], [39]. Moreover, the noise is assumed to be independent of the signal.

To proceed, it is important to clarify the modeling assumption for the signal vector $\mathbf{s}(t)$. Commonly, two primary assumptions are adopted [40]: 1) deterministic and unknown vectors, as in [41], [42], [43], and 2) Gaussian-distributed vectors, as in [3], [4], [21], [34], [44]. Both models often yield similar or even the same results in high-precision settings, such as the GLRT detectors proposed in [43] and [44]. However, when using one-bit samples, unknown deterministic models often require extra computations, making them less suited to our objectives. Therefore, for analytical simplicity, we model $\mathbf{s}(t)$ as i.i.d. ZMCSCG distribution with an unknown covariance matrix \mathbf{R}_s . Additionally, it is worth mentioning that incorporating rank information can improve detection performance, as evidenced by works in

[34], [41], [43], [44]. Nevertheless, in this study, we focus on the general case and do not impose any rank-specific constraints.

Clearly, $\mathbf{x}(t)$ follows the ZMCSCG distribution, which is determined by the population covariance matrix (PCM), defined as $\mathbf{R}_x = \mathbb{E}[\mathbf{x}(t)\mathbf{x}^H(t)]$. Under both hypotheses, the PCM is

$$\begin{aligned} \mathcal{H}_0 : \mathbf{R}_x &= \mathbf{R}_w, \\ \mathcal{H}_1 : \mathbf{R}_x &= \mathbf{H}\mathbf{R}_s\mathbf{H}^H + \mathbf{R}_w. \end{aligned} \quad (2)$$

We examine the scenario involving uncalibrated receivers, in which the covariance matrix \mathbf{R}_w is diagonal but features unequal diagonal elements. Consequently, the signal detection problem initially stated in (2) can be reformulated as:

$$\begin{aligned} \mathcal{H}_0 : \mathbf{R}_x &= \text{diag}(\sigma_{w_1}, \dots, \sigma_{w_m}), \\ \mathcal{H}_1 : \mathbf{R}_x &\neq \text{diag}(\sigma_{w_1}, \dots, \sigma_{w_m}). \end{aligned} \quad (3)$$

After one-bit quantization, the output $\mathbf{y}(t)$ is given by

$$\mathbf{y}(t) = \mathcal{Q}(\mathbf{x}(t)) = \text{sign}(\text{Re}(\mathbf{x}(t))) + \imath \text{sign}(\text{Im}(\mathbf{x}(t))), \quad (4)$$

where $\mathcal{Q}(\cdot)$ represents the one-bit quantization operator. Under each hypothesis, $\mathbf{y}(t)$ becomes

$$\begin{aligned} \mathcal{H}_0 : \mathbf{y}(t) &= \mathcal{Q}(\mathbf{w}(t)) \\ \mathcal{H}_1 : \mathbf{y}(t) &= \mathcal{Q}(\mathbf{H}\mathbf{s}(t) + \mathbf{w}(t)). \end{aligned} \quad (5)$$

The PMF of $\mathbf{y}(t)$ is given by the orthant probabilities [16]. To facilitate the computation of these orthant probabilities, we convert the received data into a real vector by concatenating its real and imaginary components:

$$\tilde{\mathbf{y}}(t) = [\text{Re}(\mathbf{y}(t))^T \quad \text{Im}(\mathbf{y}(t))^T]^T. \quad (6)$$

A similar transformation is applied to $\mathbf{x}(t)$:

$$\tilde{\mathbf{x}}(t) = [\text{Re}(\mathbf{x}(t))^T \quad \text{Im}(\mathbf{x}(t))^T]^T. \quad (7)$$

It is established in [16] that the orthant probabilities are determined only by the coherence matrix of $\tilde{\mathbf{x}}(t)$. Therefore, the hypothesis testing problem simplifies to:

$$\begin{aligned} \mathcal{H}_0 : \mathbf{P} &= \mathbf{I}_{2m}, \\ \mathcal{H}_1 : \mathbf{P} &\neq \mathbf{I}_{2m}, \end{aligned} \quad (8)$$

where $\mathbf{P} = \text{Diag}(\mathbf{R}_{\tilde{\mathbf{x}}})^{-\frac{1}{2}}\mathbf{R}_{\tilde{\mathbf{x}}}\text{Diag}(\mathbf{R}_{\tilde{\mathbf{x}}})^{-\frac{1}{2}}$ is the coherence matrix [45] of $\tilde{\mathbf{x}}(t)$, and $\mathbf{R}_{\tilde{\mathbf{x}}}$ is the PCM of $\tilde{\mathbf{x}}(t)$. Given that $\mathbf{x}(t)$ is circular, \mathbf{P} can be expressed as [46]:

$$\begin{aligned} \mathbf{P} &= \begin{bmatrix} \text{Re}(\mathbf{P}_x) & -\text{Im}(\mathbf{P}_x) \\ \text{Im}(\mathbf{P}_x) & \text{Re}(\mathbf{P}_x) \end{bmatrix} \\ &= \begin{bmatrix} \mathbf{P}_1 & \mathbf{P}_2 \\ \mathbf{P}_3 & \mathbf{P}_4 \end{bmatrix}, \end{aligned} \quad (9)$$

where \mathbf{P}_x is the coherence matrix of $\mathbf{x}(t)$. By exploiting the symmetries $\mathbf{P}_1 = \mathbf{P}_4$ and $\mathbf{P}_2 = -\mathbf{P}_3$, we effectively reduce the number of unknown parameters in \mathbf{P} to $m^2 - m$. Without loss of generality, we can define the unknown parameter vector $\boldsymbol{\theta}$ as:

$$\boldsymbol{\theta} = [\rho_{1,2}, \dots, \rho_{m-1,m}, \rho_{1+m,2}, \dots, \rho_{2m-1,m}]^T, \quad (10)$$

where ρ_{ij} is the (i, j) element of \mathbf{P} . The signal detection problem thus becomes:

$$\begin{aligned} \mathcal{H}_0 : \boldsymbol{\theta} &= \mathbf{0}, \\ \mathcal{H}_1 : \boldsymbol{\theta} &\neq \mathbf{0}. \end{aligned} \quad (11)$$

Remarkably, this paper leverages the above symmetries to minimize the number of DOFs, thereby significantly enhancing detection performance. This stands in contrast to the one-bit EMR detector presented in [22], which overlooks the signal's circularity, resulting in an over-determined system.

III. DERIVATION OF RAO'S TEST

For problems related to detection with unknown parameters, the GLRT is the most prevalent approach due to its asymptotically optimal performance and its generally good results even with limited samples [47], [48], [49]. However, when employing one-bit observations for detection, it often becomes necessary to numerically address the MLE since the likelihood function under \mathcal{H}_1 cannot be expressed in closed form. This introduces a significant computational challenge. Both Wald and Rao tests, as alternative methods to the GLRT, share the same asymptotic performance of the GLRT [47], [49], demonstrating satisfactory detection performance across various applications [40], [50], [51], [52], [53], [54], [55], [56]. However, the Wald test also requires solving the MLE under \mathcal{H}_1 . Contrasting with the first two, the Rao test circumvents the MLE solution under \mathcal{H}_1 , frequently leading to more straightforward detectors, especially when \mathcal{H}_0 is a simple hypothesis [12], [15], [47], [49]. Consequently, we opted for the Rao test in deriving our detector.

As pointed out before, to simplify the computation of the orthant probabilities, we first arrange the real and imaginary components of the observations as

$$\tilde{\mathbf{Y}} = [\tilde{\mathbf{y}}(1), \dots, \tilde{\mathbf{y}}(n)]. \quad (12)$$

It is straightforward to show that there are 2^{2m} possible values of $\tilde{\mathbf{y}}, \tilde{\mathbf{y}}^\kappa$ ($\kappa = 0, 1, \dots, 2^{2m} - 1$), where $\tilde{\mathbf{y}}$ is the sample population of $\tilde{\mathbf{y}}(t)$. Next, we define \mathbb{X}_κ as the subset of $\mathbb{R}^{2m \times 1}$ that is mapped to the one-bit quantization $\tilde{\mathbf{y}}^\kappa$ ($\kappa = 0, 1, \dots, 2^{2m} - 1$):

$$\begin{aligned} \mathbb{X}_\kappa &= \{\mathbf{x} \in \mathbb{R}^{2m \times 1} \mid \text{sign}(\mathbf{x}) = \tilde{\mathbf{y}}^\kappa\} \\ &= \{\mathbf{x} \in \mathbb{R}^{2m \times 1} \mid \text{diag}(\tilde{\mathbf{y}}^\kappa)\mathbf{x} > \mathbf{0}\}. \end{aligned} \quad (13)$$

Therefore, the probability that $\tilde{\mathbf{y}}(t) = \tilde{\mathbf{y}}^\kappa$ is

$$\begin{aligned} \Pr\{\tilde{\mathbf{y}}(t) = \tilde{\mathbf{y}}^\kappa\} &= \Pr\{\tilde{\mathbf{x}} \in \mathbb{X}_\kappa\} \\ &= \int_{\mathbb{X}_\kappa} \frac{1}{(2\pi)^m |\mathbf{R}_{\tilde{\mathbf{x}}}|^{\frac{1}{2}}} e^{-\frac{1}{2}\tilde{\mathbf{x}}^T \mathbf{R}_{\tilde{\mathbf{x}}}^{-1} \tilde{\mathbf{x}}} d\tilde{\mathbf{x}}, \end{aligned} \quad (14)$$

where $\tilde{\mathbf{x}}$ is the sample population of $\tilde{\mathbf{x}}(t)$. Consider a coordinate transformation $\tilde{\mathbf{x}} \rightarrow \tilde{\boldsymbol{\tau}} = \text{Diag}(\mathbf{R}_{\tilde{\mathbf{x}}})^{-\frac{1}{2}}\tilde{\mathbf{x}}$. Noticing that

$$\{\tilde{\boldsymbol{\tau}} \in \mathbb{R}^{2m \times 1} \mid \text{diag}(\tilde{\mathbf{y}}^\kappa)\text{Diag}(\mathbf{R}_{\tilde{\mathbf{x}}})^{\frac{1}{2}}\tilde{\boldsymbol{\tau}} > \mathbf{0}\} = \mathbb{X}_\kappa, \quad (15)$$

and the Jacobian determinant $J = |\text{Diag}(\mathbf{R}_{\tilde{\mathbf{x}}})^{\frac{1}{2}}|$, (14) can be written as

$$\Pr\{\tilde{\mathbf{y}}(t) = \tilde{\mathbf{y}}^\kappa\} = \int_{\mathbb{X}_\kappa} \frac{1}{(2\pi)^m |\mathbf{P}|^{\frac{1}{2}}} e^{-\frac{1}{2}\tilde{\boldsymbol{\tau}}^T \mathbf{P}^{-1} \tilde{\boldsymbol{\tau}}} d\tilde{\boldsymbol{\tau}}. \quad (16)$$

Defining the vector $\zeta_\kappa = \text{diag}(\tilde{\mathbf{y}}^\kappa)\tilde{\boldsymbol{\tau}}$, we have

$$\begin{aligned} \Pr\{\tilde{\mathbf{y}}(t) = \tilde{\mathbf{y}}^\kappa\} &= \int_0^\infty \cdots \int_0^\infty \frac{1}{(2\pi)^m |\mathbf{P}|^{\frac{1}{2}}} e^{-\frac{1}{2}\zeta_\kappa^T \mathbf{S}_\kappa^{-1} \zeta_\kappa} d\zeta_\kappa \\ &= \int_0^\infty \cdots \int_0^\infty \frac{1}{(2\pi)^m |\mathbf{P}|^{\frac{1}{2}}} e^{-\frac{1}{2}\mathbf{x}^T \mathbf{S}_\kappa^{-1} \mathbf{x}} d\mathbf{x}, \end{aligned} \quad (17)$$

where

$$\mathbf{S}_\kappa = \text{diag}(\tilde{\mathbf{y}}^\kappa)\mathbf{P}\text{diag}(\tilde{\mathbf{y}}^\kappa). \quad (18)$$

Since $|\mathbf{S}_\kappa| = |\mathbf{P}|$, $\Pr\{\tilde{\mathbf{y}}(t) = \tilde{\mathbf{y}}^\kappa\}$ can be rewritten as

$$\Pr\{\tilde{\mathbf{y}}(t) = \tilde{\mathbf{y}}^\kappa\} = \phi[\mathbf{S}_\kappa], \quad (19)$$

where

$$\phi[\boldsymbol{\Sigma}] = \int_0^\infty \cdots \int_0^\infty \frac{1}{(2\pi)^m |\boldsymbol{\Sigma}|^{\frac{1}{2}}} e^{-\frac{1}{2}\mathbf{x}^T \boldsymbol{\Sigma}^{-1} \mathbf{x}} d\mathbf{x}, \quad (20)$$

is the central orthant probability.

Therefore, the likelihood function of $\tilde{\mathbf{Y}}$ is

$$p(\tilde{\mathbf{Y}}; \boldsymbol{\theta}) = \prod_{t=1}^n p(\tilde{\mathbf{y}}(t); \boldsymbol{\theta}) = \prod_{t=1}^n \phi[\mathbf{S}(t)], \quad (21)$$

where $p(\tilde{\mathbf{y}}(t); \boldsymbol{\theta})$ is the PMF of $\tilde{\mathbf{y}}(t)$ and

$$\mathbf{S}(t) = \text{diag}(\tilde{\mathbf{y}}(t))\mathbf{P}\text{diag}(\tilde{\mathbf{y}}(t)). \quad (22)$$

Hence, the log-likelihood function can be expressed as

$$\mathcal{L}(\tilde{\mathbf{Y}}; \boldsymbol{\theta}) = \sum_{t=1}^n \log(\phi[\mathbf{S}(t)]). \quad (23)$$

Once we have derived the log-likelihood, the statistic of Rao's test is computed as

$$T_R = \left(\frac{\partial \mathcal{L}(\tilde{\mathbf{Y}}; \boldsymbol{\theta})}{\partial \boldsymbol{\theta}} \bigg|_{\boldsymbol{\theta}=\boldsymbol{\theta}_0} \right)^T \mathbf{F}^{-1}(\boldsymbol{\theta}_0) \left(\frac{\partial \mathcal{L}(\tilde{\mathbf{Y}}; \boldsymbol{\theta})}{\partial \boldsymbol{\theta}} \bigg|_{\boldsymbol{\theta}=\boldsymbol{\theta}_0} \right), \quad (24)$$

where $\boldsymbol{\theta}_0 = \mathbf{0} \in \mathbb{R}^{(m^2-m) \times 1}$ corresponds to the parameters under \mathcal{H}_0 and $\mathbf{F}(\boldsymbol{\theta})$ is the Fisher information matrix (FIM), which is defined as

$$\mathbf{F}(\boldsymbol{\theta}) = \mathbb{E} \left[\frac{\partial \mathcal{L}(\tilde{\mathbf{Y}}; \boldsymbol{\theta})}{\partial \boldsymbol{\theta}} \frac{\partial \mathcal{L}(\tilde{\mathbf{Y}}; \boldsymbol{\theta})}{\partial \boldsymbol{\theta}^T} \right]. \quad (25)$$

The result of (24) is provided by the following theorem.

Theorem 1: The Rao's test corresponding to the hypothesis testing problem (11) is given by

$$T_R = \frac{n}{2} \sum_{\substack{i,j=1 \\ i < j}}^m |\hat{r}_{ij}|^2, \quad (26)$$

where \hat{r}_{ij} is the (i, j) element of the complex-valued one-bit sample covariance matrix (SCM):

$$\hat{\mathbf{R}}_{\mathbf{y}} = \frac{1}{n} \sum_{t=1}^n \mathbf{y}(t)\mathbf{y}^H(t). \quad (27)$$

Proof: See Appendix A. \square

Hence, the detection algorithm based on Rao's test is

$$T_R \underset{\mathcal{H}_0}{\overset{\mathcal{H}_1}{\geq}} \gamma_R, \quad (28)$$

where γ_R represents the threshold.

Moreover, recall that the second-order ∞ -bit EMR detector [21] is

$$T_{\text{EMR}}(\hat{\mathbf{R}}_{\mathbf{x}}) = \frac{\frac{1}{m} \|\hat{\mathbf{R}}_{\mathbf{x}}\|^2}{\left(\frac{1}{m} \text{tr}(\hat{\mathbf{R}}_{\mathbf{x}})\right)^2} \underset{\mathcal{H}_0}{\overset{\mathcal{H}_1}{\geq}} \gamma_{\text{EMR}}. \quad (29)$$

Here, $\hat{\mathbf{R}}_{\mathbf{x}}$ is the SCM calculated from the unquantized samples $\mathbf{X} = [\mathbf{x}(1), \dots, \mathbf{x}(n)]$. Utilizing the fact that the diagonal elements of $\hat{\mathbf{R}}_{\mathbf{y}}$ are 2, we have

$$T_{\text{EMR}}(\hat{\mathbf{R}}_{\mathbf{y}}) = \frac{1}{mn} T_R + 1. \quad (30)$$

This implies that the Rao's test is equivalent to the EMR test employing the complex-valued one-bit SCM. It is important to note that this result is distinct from the one presented in [22]. In that study, the EMR detector is specifically employed by submitting the expanded real-valued one-bit SCM, denoted as $\hat{\mathbf{R}}_{\tilde{\mathbf{y}}}$, into the calculation. This $\hat{\mathbf{R}}_{\tilde{\mathbf{y}}}$ is defined as follows:

$$\hat{\mathbf{R}}_{\tilde{\mathbf{y}}} = \frac{1}{n} \sum_{t=1}^n \tilde{\mathbf{y}}(t)\tilde{\mathbf{y}}(t)^T. \quad (31)$$

IV. DISTRIBUTIONS OF PROPOSED TEST

In this section, we first analyze the constant false alarm rate (CFAR) characteristic of the proposed detector. Subsequently, the asymptotic distributions of T_R under \mathcal{H}_0 and \mathcal{H}_1 are derived. Since T_R is bounded on $[0, nm(m-1)]$, we can choose a Beta distribution to approximate its distribution, after a proper normalization. The approximation is conducted by first computing the first- and second-order moments of the detector and then matching them with that of the Beta distribution to determine the parameters.

A. CFAR Property

We employ invariance theory to evaluate the CFAR characteristic of the proposed detector. Consider $\boldsymbol{\Sigma}'$ as a diagonal matrix with unknown and positive diagonal elements. To establish the CFAR property, it is essential to demonstrate two points under \mathcal{H}_0 [40], [57]:

- 1) The one-bit quantization of the transformation $\boldsymbol{\Sigma}'^{\frac{1}{2}} \mathbf{x}(t)$, denoted as $\mathcal{Q}(\boldsymbol{\Sigma}'^{\frac{1}{2}} \mathbf{x}(t))$, belongs to the same distribution family as the original one-bit data $\mathbf{y}(t)$.
- 2) The detector processes $\mathcal{Q}(\boldsymbol{\Sigma}'^{\frac{1}{2}} \mathbf{x}(t))$ to yield the same result as with $\mathbf{y}(t)$.

Given that $\boldsymbol{\Sigma}'$ is diagonal with positive diagonal elements, and using $\text{sign}(ax) = \text{sign}(x)$, for $a > 0$, we obtain:

$$\begin{aligned} \mathcal{Q}(\boldsymbol{\Sigma}'^{\frac{1}{2}} \mathbf{x}(t)) &= \text{sign}(\boldsymbol{\Sigma}'^{\frac{1}{2}} \text{Re}(\mathbf{x}(t))) + \imath \text{sign}(\boldsymbol{\Sigma}'^{\frac{1}{2}} \text{Im}(\mathbf{x}(t))) \\ &= \text{sign}(\text{Re}(\mathbf{x}(t))) + \imath \text{sign}(\text{Im}(\mathbf{x}(t))) \\ &= \mathbf{y}(t). \end{aligned} \quad (32)$$

This equation confirms that $\mathcal{Q}(\Sigma'^{\frac{1}{2}}\mathbf{x}(t))$ is identically equal to $\mathbf{y}(t)$, implying that both share the same distribution. Additionally, we have:

$$\begin{aligned} T_{\mathbf{R}}(\mathcal{Q}(\Sigma'^{\frac{1}{2}}\mathbf{X})) &= \frac{n}{2} \sum_{\substack{i,j=1 \\ i < j}}^m \left| \frac{1}{n} \sum_{t=1}^n \mathcal{Q}(\sigma_i' x_i(t)) \mathcal{Q}(\sigma_j' x_j(t))^* \right|^2 \\ &= \frac{n}{2} \sum_{\substack{i,j=1 \\ i < j}}^m \left| \frac{1}{n} \sum_{t=1}^n y_i(t) y_j^*(t) \right|^2 \\ &= T_{\mathbf{R}}(\mathbf{Y}), \end{aligned} \quad (33)$$

where $\mathbf{Y} = [\mathbf{y}(1), \dots, \mathbf{y}(n)]$, and $(\sigma_i')^2$ is the (i, i) of the Σ' .

Recall that the expression of the one-bit EMR [22] is

$$T_{\mathbf{O}} = 1 + \frac{1}{m} \sum_{\substack{i,j=1 \\ i < j}}^{2m} |\hat{r}_{\tilde{\mathbf{y}}}(i, j)|^2, \quad (34)$$

where $\hat{r}_{\tilde{\mathbf{y}}}(i, j)$ represents the (i, j) element of the expanded real-valued one-bit SCM $\hat{\mathbf{R}}_{\tilde{\mathbf{y}}}$. Let us define $\tilde{\mathbf{y}}_{\text{tra}}(t)$ to represent the expand real-valued one-bit quantization of the transform $\Sigma'^{\frac{1}{2}}\mathbf{x}(t)$, given by

$$\tilde{\mathbf{y}}_{\text{tra}}(t) = [\text{Re}(\mathcal{Q}(\Sigma'^{\frac{1}{2}}\mathbf{x}(t)))^T \text{Im}(\mathcal{Q}(\Sigma'^{\frac{1}{2}}\mathbf{x}(t)))^T]^T. \quad (35)$$

Since

$$\hat{\mathbf{R}}_{\tilde{\mathbf{y}}_{\text{tra}}} = \frac{1}{n} \sum_{t=1}^n \tilde{\mathbf{y}}_{\text{tra}}(t) \tilde{\mathbf{y}}_{\text{tra}}(t)^T = \frac{1}{n} \sum_{t=1}^n \tilde{\mathbf{y}}(t) \tilde{\mathbf{y}}(t)^T = \hat{\mathbf{R}}_{\tilde{\mathbf{y}}}, \quad (36)$$

we have

$$T_{\mathbf{O}}(\mathcal{Q}(\Sigma'^{\frac{1}{2}}\mathbf{X})) = T_{\mathbf{O}}(\mathbf{Y}). \quad (37)$$

The derivations provided above show that the proposed method and the one-bit EMR maintain a constant detection threshold even when the noise variances change. Consequently, both approaches are CFAR under conditions of noise variance uncertainty. These CFAR characteristics are also verified with simulations in Section VI.

B. Distribution Under \mathcal{H}_0

To project the detector to the interval of $[0, 1]$, we define a new statistic

$$T_{\mathbf{R}}' = \frac{1}{nm(m-1)} T_{\mathbf{R}}, \quad (38)$$

whose first and second-order moments of $T_{\mathbf{R}}'$ under \mathcal{H}_0 are given in the following theorem.

Theorem 2: Under \mathcal{H}_0 , $T_{\mathbf{R}}'$ has mean

$$\mu_0 = \frac{1}{n}, \quad (39)$$

and variance

$$\sigma_0^2 = \frac{2(n-1)}{m(m-1)n^3}. \quad (40)$$

Proof: See Appendix B. \square

The cumulative distribution function (CDF) of the Beta distribution is

$$F(x; \alpha, \beta) = \frac{\Gamma(\alpha + \beta)}{\Gamma(\alpha)\Gamma(\beta)} B(x; \alpha, \beta), \quad (41)$$

where the incomplete Beta function is

$$B(x; \alpha, \beta) = \int_0^x z^{\alpha-1} (1-z)^{\beta-1} dz, \quad (42)$$

and $\Gamma(x) = \int_0^{+\infty} t^{x-1} e^{-t} dt$, for $x > 0$, is the Gamma function. In addition, the mean and variance of a Beta distribution can be calculated as

$$\mu = \frac{\alpha}{\alpha + \beta}, \quad \sigma^2 = \frac{\alpha\beta}{(\alpha + \beta)^2(\alpha + \beta + 1)}. \quad (43)$$

Matching (43) with (39) and (40), we obtain the approximated null distribution of $T_{\mathbf{R}}'$:

$$\Pr\{T_{\mathbf{R}}' < \gamma\} \approx \frac{\Gamma(\alpha_0 + \beta_0)}{\Gamma(\alpha_0)\Gamma(\beta_0)} B(\gamma; \alpha_0, \beta_0), \quad (44)$$

where

$$\alpha_0 = \frac{nm(m-1) - 2}{2n}, \quad (45)$$

$$\beta_0 = \frac{(n-1)[nm(m-1) - 2]}{2n}. \quad (46)$$

C. Distribution Under \mathcal{H}_1

Under \mathcal{H}_1 , the mean and variance of $T_{\mathbf{R}}'$ are given by the following theorem.

Theorem 3: Under \mathcal{H}_1 , the mean of $T_{\mathbf{R}}'$ is

$$\mu_1 = \frac{1}{2m(m-1)} \sum_{\substack{i,j=1 \\ i < j}}^m g_{ij}, \quad (47)$$

and the variance of $T_{\mathbf{R}}'$ is

$$\sigma_1^2 = \frac{1}{4m^2(m-1)^2} \sum_{\substack{i,j,k,l=1 \\ i < j, k < l}}^m (f_{ijkl} - g_{ijkl}), \quad (48)$$

where g_{ij} , f_{ijkl} , and g_{ijkl} are defined in Appendix C.

Proof: See Appendix C. \square

Similar to \mathcal{H}_0 , the CDF of $T_{\mathbf{R}}'$ under \mathcal{H}_1 can be approximated by a Beta distribution as

$$\Pr\{T_{\mathbf{R}}' < \gamma\} \approx \frac{\Gamma(\alpha_1 + \beta_1)}{\Gamma(\alpha_1)\Gamma(\beta_1)} B(\gamma; \alpha_1, \beta_1), \quad (49)$$

where

$$\alpha_1 = \frac{\mu_1(\mu_1 - \mu_1^2 - \sigma_1^2)}{\sigma_1^2}, \quad (50)$$

$$\beta_1 = \frac{(1 - \mu_1)(\mu_1 - \mu_1^2 - \sigma_1^2)}{\sigma_1^2}. \quad (51)$$

V. ANALYSIS OF PERFORMANCE DEGRADATION

In this section, we investigate the degradation in detection performance when using one-bit ADCs in comparison to ∞ -bit ADCs. Note that the ∞ -bit EMR belongs to the category of sphericity tests, which consider both the independence between the random variables and the equality of their variances. However, due to the loss of amplitude information in the one-bit context, it becomes impossible to compare the variances. Thus, we choose to compare our result with the locally most powerful invariant test (LMPIT) for independence in [33]. In fact, when the SNR is low, the diagonal entries of the covariance matrix tend to be close to each other, resulting in the sphericity test delivering performance very close to that of the independence test, as demonstrated by simulations in [58].

A. ∞ -Bit Case

The detection problem for ∞ -bit ADCs is (3). The LMPIT for this problem is [33]

$$T_L = ntr \left(\left(\hat{\mathbf{R}}_x \text{Diag}(\hat{\mathbf{R}}_x)^{-1} - \mathbf{I}_m \right)^2 \right) \underset{\mathcal{H}_0}{\overset{\mathcal{H}_1}{\gtrless}} \gamma_L, \quad (52)$$

and its asymptotic distribution has been analyzed [30]:

$$T_L \sim \begin{cases} \chi_k^2, & \text{under } \mathcal{H}_0, \\ \chi_k^2(\delta_\infty^2), & \text{under } \mathcal{H}_1, \end{cases} \quad (53)$$

where $k = m^2 - m$ and $\delta_\infty^2 = ntr[(\mathbf{P}_x - \mathbf{I}_m)^2] = 2n\|\boldsymbol{\theta}\|^2$.

B. One-Bit Case

In Section IV, we exploit the Beta distribution to approximate the distribution of T_R . However, it is difficult to use it to compare with the ∞ -bit detectors to analyze the performance degradation. Therefore, we choose to derive a new approximate distribution of T_R in the low-SNR regime in terms of non-central χ^2 distribution. First, we rewrite T_R as

$$T_R = \|\tilde{\mathbf{r}}_{sc}\|^2, \quad (54)$$

where $\tilde{\mathbf{r}}_{sc} = \sqrt{\frac{n}{2}}\tilde{\mathbf{r}}$. Here, we remind the reader that $\tilde{\mathbf{r}} = [\text{Re}(\hat{\mathbf{r}})^T, \text{Im}(\hat{\mathbf{r}})^T]^T$, and $\hat{\mathbf{r}}$ is defined in (76). The asymptotic distribution of $\tilde{\mathbf{r}}_{sc}$ is presented next.

Theorem 4: In the low-SNR regime where $\boldsymbol{\theta}$ is of order $\mathcal{O}(n^{-\frac{1}{2}})$, the random vector $\tilde{\mathbf{r}}_{sc}$ asymptotically follows a multi-dimensional real Gaussian distribution with mean

$$\mathbb{E}[\tilde{\mathbf{r}}_{sc}] = \frac{2\sqrt{2n}}{\pi}\boldsymbol{\theta} + \mathcal{O}(n^{-\frac{1}{2}}), \quad (55)$$

and covariance matrix

$$\mathbf{R}_{\tilde{\mathbf{r}}_{sc}} = \mathbf{I}_{m^2-m} + \mathcal{O}(n^{-\frac{1}{2}}). \quad (56)$$

Proof: See Appendices D and E. \square

Using the above results, it is easy to conclude that

$$T_R \sim \begin{cases} \chi_k^2, & \text{under } \mathcal{H}_0, \\ \chi_k^2(\delta_1^2), & \text{under } \mathcal{H}_1, \end{cases} \quad (57)$$

where

$$\delta_1^2 = \frac{8n}{\pi^2} \|\boldsymbol{\theta}\|^2 = \frac{4}{\pi^2} \delta_\infty^2. \quad (58)$$

Therefore, we can deduce that the performance degradation in the low SNR is approximately $10 \log_{10}(\sqrt{\delta_\infty^2/\delta_1^2}) \approx 2$ dB. Alternatively, this performance loss can be compensated by increasing the sample support by about $\delta_\infty^2/\delta_1^2 = \pi^2/4 \approx 2.47$ times more samples.

Remark 1: It is worth noting that in [12], the 2 dB loss requires only $\pi/2 \approx 1.57$ times more samples to compensate. When compared with the results in this paper, it becomes evident that the efficiency of non-coherent accumulation is the square root of that of coherent accumulation.

VI. NUMERICAL RESULTS

In this section, Monte Carlo experiments are conducted. Firstly, we evaluate the CFAR characteristic of our detector. We then assess the accuracy of the detector distribution that we have derived under different SNRs. Subsequently, we compare the performance of our detector with that of the one-bit EMR [22]. Finally, we verify our theoretical analysis by demonstrating that the performance degradation is as low as 2 dB.

We conduct 10^6 Monte Carlo trials for all experiments. The SNR is defined as:

$$\text{SNR} = 10 \log_{10} \left(\frac{\bar{\sigma}_s^2}{\bar{\sigma}_w^2} \right). \quad (59)$$

where $\bar{\sigma}_s^2 = \text{tr}(\mathbf{R}_s)/p$ and $\bar{\sigma}_w^2 = \text{tr}(\mathbf{R}_w)/m$.

We further assess the distribution accuracy of our approximations through the Cramér-von Mises goodness-of-fit criterion. This statistical measure is frequently employed to measure the fidelity of a given distribution, especially in specialized fields like the analysis of clutter data [59], [60], [61]. The criterion is defined as:

$$\epsilon = \frac{1}{K} \sum_{i=1}^K \left| F(\xi_i) - \hat{F}(\xi_i) \right|^2, \quad (60)$$

where K is the number of thresholds sampled, ξ_i is the i th threshold value, and $F(\xi_i)$ and $\hat{F}(\xi_i)$ are empirical and approximate CDFs, respectively.

A. Null Distribution

We first evaluate CFAR properties of proposed detector and one-bit EMR detector [22]. We set $m=4$, $n=128$ and $[\sigma_{w_1}, \sigma_{w_2}, \sigma_{w_3}, \sigma_{w_4}] = [1, 1, 1, 1]$, $[0.4, 0.8, 1.2, 1.6]$, and $[0.5, 0.75, 1.2, 1.5]$. The results are depicted in Fig. 1. It is worth noting that, to ensure that the one-bit EMR detector and the proposed detector operate within a similar range, we have scaled the one-bit EMR as $T'_O = mn(T_O - 1)$. Fig. 1 indicates that both our detector and the one-bit EMR detector exhibit CFAR properties, which are consistent with the analytical results discussed in Section IV.

Then, we examine the accuracy of the null distribution of the proposed detector. Its approximate distributions include (44) and (57). The simulation results are plotted in Fig. 2. We set

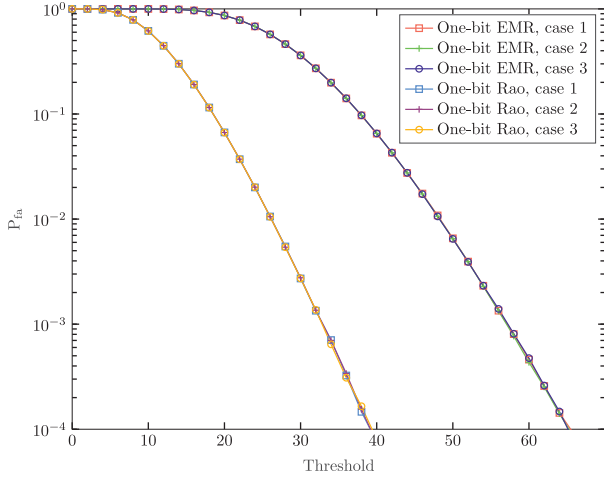


Fig. 1. Probability of false alarm versus threshold for $m = 4$, $n = 128$ and ‘case1’, ‘case2’, and ‘case3’ correspond to $[\sigma_{w_1}, \sigma_{w_2}, \sigma_{w_3}, \sigma_{w_4}] = [1, 1, 1, 1]$, $[0.4, 0.8, 1.2, 1.6]$, and $[0.5, 0.75, 1.2, 1.5]$, respectively.

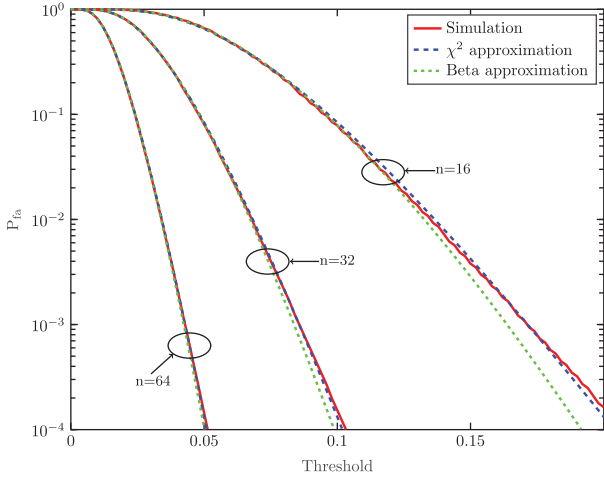


Fig. 2. Probability of false alarm versus threshold for $m = 4$ and $n = 16, 32$, and 64 .

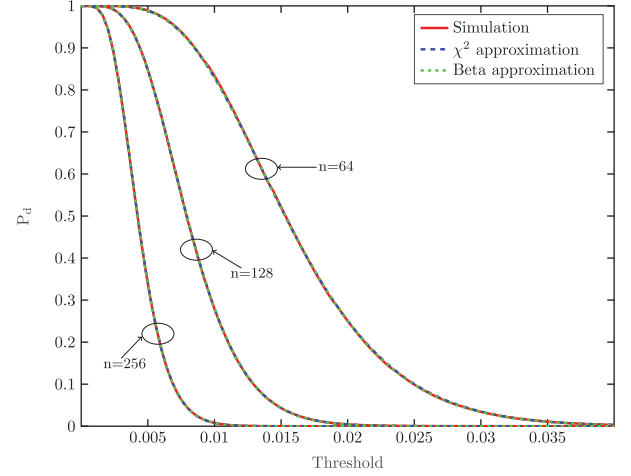
$m = 4$ and $n = 16, 32$ and 64 . It is worth noting that T'_R , defined in (38), is used, since it belongs to the interval of $[0, 1]$. Simultaneously, the result in (57) is normalized by setting $\gamma' = \gamma/[mn(m-1)]$. Fig. 2 reveals that, for $n = 16$, both the Beta and χ^2 distributions fit the empirical distribution well at large values of P_{fa} . However, the χ^2 distribution demonstrates better fitting at small values of P_{fa} . As n increases, both the Beta and χ^2 distributions progressively align more closely with the empirical distribution, reaching a satisfactory level of fit when $n = 64$. This observation is further corroborated by the approximate error in Table I, which also suggests that the Beta distribution generally provides a better overall fit compared to the χ^2 distribution.

B. Non-Null Distribution

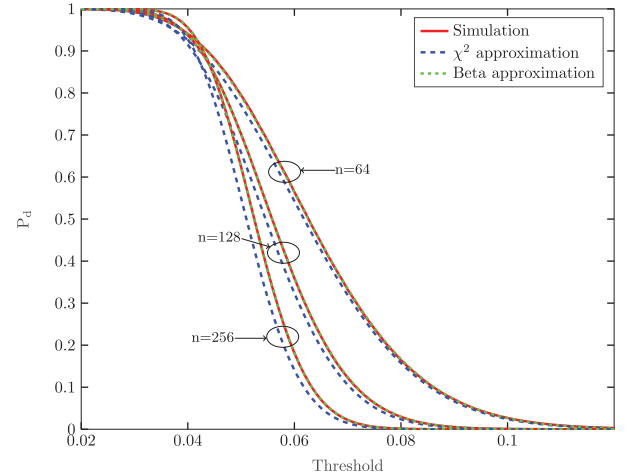
In this section, we investigate the accuracy of the approximate non-null distribution of the proposed detector, which

TABLE I
ERRORS OF NULL DISTRIBUTION APPROXIMATIONS

Approximation	$m = 4$		
	$n = 16$	$n = 32$	$n = 64$
(44)	1.55×10^{-5}	1.91×10^{-6}	2.78×10^{-7}
(57)	3.61×10^{-5}	4.32×10^{-6}	5.69×10^{-7}



(a) SNR = -9 dB



(b) SNR = 4 dB

Fig. 3. Probability of detection versus threshold for $m = 4$, $p = 2$ and $n = 64, 128$, and 256 .

includes (49) and (57). The parameters are set as $m = 4$, $p = 2$, $n = 64, 128, 256$, and SNR = -9 dB, 4 dB. To increase reproducibility, we specify our channel matrix as:

$$\mathbf{H} = \begin{bmatrix} 0.5282 - i0.0658 & -0.3370 - i0.4516 \\ 0.0294 + i0.3040 & 0.7462 + i0.1550 \\ -0.5102 - i0.2616 & -0.1954 - i0.0563 \\ -0.2539 - i0.4797 & 0.2375 - i0.0622 \end{bmatrix}.$$

Fig. 3(a) demonstrates that, in the low SNR regime, both approximations effectively fit the empirical distributions. In contrast, Fig. 3(b) indicates that, in the high SNR regime, the

TABLE II
ERRORS OF NON-NULL DISTRIBUTION APPROXIMATIONS AT DIFFERENT SNRS

Approximation	SNR = -9 dB, $m = 4, p = 2$			SNR = 4 dB, $m = 4, p = 2$		
	$n = 64$	$n = 128$	$n = 256$	$n = 64$	$n = 128$	$n = 256$
(49)	1.30×10^{-6}	1.99×10^{-7}	2.03×10^{-8}	1.92×10^{-6}	4.93×10^{-7}	9.23×10^{-8}
(57)	2.55×10^{-6}	2.56×10^{-7}	5.69×10^{-8}	1.60×10^{-4}	4.07×10^{-4}	7.91×10^{-4}

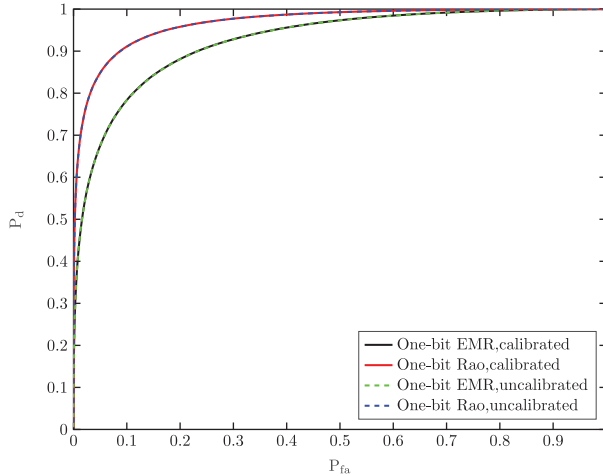


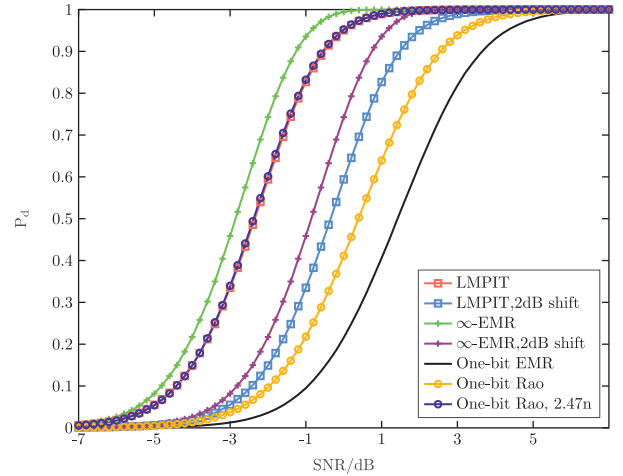
Fig. 4. Empirical ROCs for $m = 4, p = 2, n = 128$ and SNR = -1dB.

distribution in (49) maintains a good fit with the empirical distribution, whereas the distribution in (57) does not exhibit a satisfactory accuracy. The asymptotic errors, as presented in Table II, support these observations.

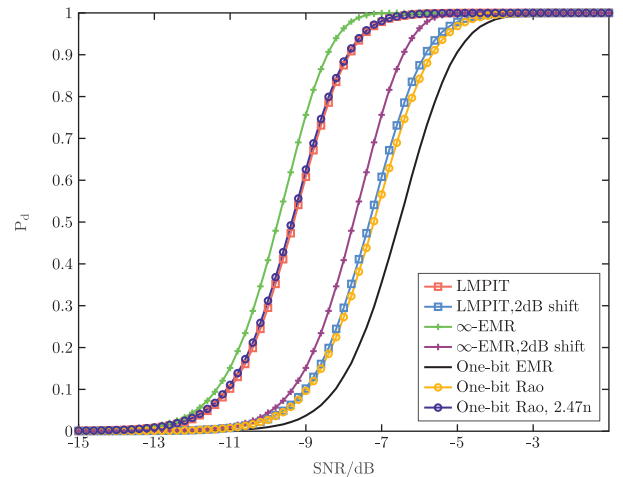
The reason for these differences in accuracy is that the Beta distribution in (49) is obtained via the method of moments without imposing restrictions on the SNR. Conversely, the non-central χ^2 distribution in (57) is derived under the assumption of a low SNR regime, which explains its diminished accuracy in the high SNR context.

C. Detection Performance

In this simulation, we evaluate the performance of the proposed detector by comparing it with the one-bit EMR detector outlined in [22], and specified by (34), through receiver operating characteristic (ROC) curves. For this experiment, we set the parameters as $m = 4, p = 2, n = 128$ and SNR = -1 dB. The channel matrix \mathbf{H} is set as the same as previous subsection. Moreover, we explore the impact of receiver calibration by employing two distinct sets of noise variances. In one scenario, we uniformly assign a noise variance of 1 to all receivers. In the alternative scenario, the noise variances are set as $[\sigma_{w_1}, \sigma_{w_2}, \sigma_{w_3}, \sigma_{w_4}] = [0.4, 0.8, 1.2, 1.6]$, thereby maintaining the total noise power constant across both cases. As depicted in Fig. 4, our proposed method demonstrates superior performance compared to the one-bit EMR detector. Additionally, it is noteworthy that the performance of both the one-bit EMR detector and our proposed detector remain the same in calibrated and uncalibrated scenarios.



(a) $n = 128$



(b) $n = 2048$

Fig. 5. Probability of detection versus SNR for $P_{fa} = 10^{-4}, m = 4$ and $p = 2$.

D. Performance Degradation

In this section, we analyze the performance gap between the proposed one-bit detector and existing ∞ -bit detectors. We maintain a fixed false alarm probability of $P_{fa} = 10^{-4}$ and examine how the detection probabilities vary with SNR. The parameters are set as $m = 4, p = 2$, and $n = [128, 2048]$. To account for the potential impact of the choice of \mathbf{H} on detection performance, a weighted evaluation approach is employed. Specifically, during each trial, \mathbf{H} is randomly generated through a ZMCSCG distribution and its columns are subsequently normalized. The results are displayed in Fig. 5. It can be

observed that with the same number of samples, the performance degradation of our proposed detector is less than that of the one-bit EMR detector. In addition, Fig. 5(a) reveals that when n is not sufficiently large, the performance gap between our detector and the LMPIT exceeds 2 dB. Conversely, Fig. 5(b) suggests that at lower SNR values and larger n , the performance degradation of our detector compared to LMPIT is approximately 2 dB. This observation aligns with the theoretical derivations presented in Section V. Moreover, as SNR declines, the performance gap between our detector and the ∞ -bit EMR also narrows, although it remains slightly above 2 dB. This is because ∞ -bit EMR additionally considers the equality of noise variances. With the loss of amplitude information in one-bit sampling, this property no longer contributes to the detection power, thereby slightly amplifying the performance shortfall beyond 2 dB.

Fig. 5 further reveals that, when using $2.47n$ samples, the performance curve of our proposed detector aligns exceptionally well with that of LMPIT in both subfigures. Particularly, in Fig. 5(a), a gap exists between the curve of our detector and LMPIT with 2 dB shift, while the curve of the proposed detector with $2.47n$ samples aligns closely with the LMPIT curve. This underscores the pivotal role of sample size in validating the analytical framework presented in (57) to hold.

VII. CONCLUSION

In this paper, a closed-form detector based on Rao's test for blind spectrum sensing utilizing one-bit observations is proposed. We derive its null and non-null distributions using the method of moments, allowing us to calculate its false alarm and detection probabilities. Furthermore, the performance degradation of the proposed detector in comparison to the LMPIT detector using ∞ -bit observations is examined. Through our analysis, we determine that the performance degradation is about 2 dB in the low SNR regime. To compensate for this performance degradation, the sampling number of one-bit observations can be increased by approximately 2.47 times. Additionally, we find that the effectiveness of non-coherent detection is the square root of coherent detection.

As future work, this approach can be generalized to one-bit sampling with time-varying thresholds in order to incorporate the diagonal elements of the covariance matrix, which could further enhance the detection performance.

APPENDIX A PROOF OF THEOREM 1

To obtain T_R , we first need to compute the partial derivative of the log-likelihood function with respect to the unknown parameters at $\boldsymbol{\theta} = \boldsymbol{\theta}_0 = \mathbf{0}$.

Using (23), it is easy to show that

$$\begin{aligned} \mathcal{L}(\tilde{\mathbf{Y}}; \boldsymbol{\theta} = \mathbf{0}) &= \sum_{t=1}^n \log(\phi[\mathbf{I}_{2m}]) = \sum_{t=1}^n \log\left(\left(\frac{1}{2}\right)^{2m}\right) \\ &= -2mn \log(2). \end{aligned} \quad (61)$$

Now, we rewrite the orthant probability $\phi[\boldsymbol{\Sigma}]$ by the coordinate transformation $\mathbf{x} \rightarrow \mathbf{y} = \mathbf{E}_{ab}\mathbf{x}$, where $a, b = 1, \dots, 2m$

and \mathbf{E}_{ab} is obtained by swapping i th row and j th row of the identity matrix. It is easy to get the Jacobian determinant $J' = |\mathbf{E}_{ab}|$ due to $\mathbf{E}_{ab}^{-1} = \mathbf{E}_{ab}$. Since $|\mathbf{E}_{ab}| = -1$ for $a = b$ and $|\mathbf{E}_{ab}| = 1$ for $a \neq b$, the absolute value of the Jacobian determinant is in all cases 1. Thus, $\phi[\boldsymbol{\Sigma}]$ can be calculated by

$$\phi[\boldsymbol{\Sigma}] = \int_0^\infty \cdots \int_0^\infty \frac{1}{(2\pi)^m |\boldsymbol{\Sigma}|^{\frac{1}{2}}} e^{-\frac{1}{2}\mathbf{y}^T(\mathbf{E}_{ab}\boldsymbol{\Sigma}\mathbf{E}_{ab})^{-1}\mathbf{y}} d\mathbf{y}. \quad (62)$$

Noticing that $|\mathbf{E}_{ab}\boldsymbol{\Sigma}\mathbf{E}_{ab}| = |\boldsymbol{\Sigma}|$, we have

$$\phi[\boldsymbol{\Sigma}] = \phi[\mathbf{E}_{ab}\boldsymbol{\Sigma}\mathbf{E}_{ab}]. \quad (63)$$

Define that $\mathbf{T}_1(i, j) = \mathbf{E}_{4,j'}\mathbf{E}_{3,i'}\mathbf{E}_{2,j}\mathbf{E}_{1,i}$, where $1 \leq i < j \leq m$ and $\{i', j'\} = \{i, j\} + m$, using (63), we can obtain $\phi[\mathbf{S}(t)]$ as

$$\phi[\mathbf{S}(t)] = \phi[\mathbf{T}_1(i, j)\mathbf{S}(t)\mathbf{T}_1^T(i, j)]. \quad (64)$$

For $\boldsymbol{\theta} = \boldsymbol{\theta}_{i,j}$, where $\boldsymbol{\theta}_{a,b}$ is obtained by zeroing out the elements of $\boldsymbol{\theta}$ except ρ_{ab} , $\mathbf{T}_1(i, j)\mathbf{S}(t)\mathbf{T}_1^T(i, j)$ can be expressed as

$$\mathbf{T}_1(i, j)\mathbf{S}(t)\mathbf{T}_1^T(i, j) = \begin{bmatrix} \mathbf{S}_{ij}(t) & \mathbf{0} & \mathbf{0} \\ \mathbf{0} & \mathbf{S}_{i'j'}(t) & \mathbf{0} \\ \mathbf{0} & \mathbf{0} & \mathbf{I}_{2m-4} \end{bmatrix}, \quad (65)$$

where

$$\mathbf{S}_{ab}(t) = \begin{bmatrix} 1 & \tilde{y}_a(t)\tilde{y}_b(t)\rho_{ab} \\ \tilde{y}_a(t)\tilde{y}_b(t)\rho_{ab} & 1 \end{bmatrix}. \quad (66)$$

Substituting (65) into (64), we get that

$$\phi[\mathbf{S}(t)]|_{\boldsymbol{\theta}=\boldsymbol{\theta}_{i,j}} = \phi[\mathbf{S}_{ij}(t)]\phi[\mathbf{S}_{i'j'}(t)]\phi[\mathbf{I}_{2m-4}], \quad (67)$$

since the elements of Gaussian vector corresponding to different diagonal blocks of the coherence matrix are independent. Similarly, for $\boldsymbol{\theta} = \boldsymbol{\theta}_{i',j}$, we have

$$\begin{aligned} \phi[\mathbf{S}(t)]|_{\boldsymbol{\theta}=\boldsymbol{\theta}_{i',j}} &= \phi[\mathbf{T}_2(i, j)\mathbf{S}(t)\mathbf{T}_2^T(i, j)] \\ &= \phi[\mathbf{S}_{i'j}(t)]\phi[\mathbf{S}_{ij'}(t)]\phi[\mathbf{I}_{2m-4}] \end{aligned} \quad (68)$$

where $\mathbf{T}_2(i, j) = \mathbf{E}_{4,j'}\mathbf{E}_{3,i}\mathbf{E}_{2,j}\mathbf{E}_{1,i'}$. Moreover, each $\phi[\mathbf{S}_{ab}(t)]$ is the integral in the positive quadrant of a zero-mean bi-dimensional Gaussian with covariance matrix $\mathbf{S}_{ab}(t)$, which can be calculated by [62]

$$\phi[\mathbf{S}_{ab}(t)] = \frac{1}{4} + \frac{1}{2\pi} \arcsin[\tilde{y}_a(t)\tilde{y}_b(t)\rho_{ab}]. \quad (69)$$

Therefore, we have

$$\begin{aligned} \mathcal{L}(\tilde{\mathbf{Y}}; \boldsymbol{\theta} = \boldsymbol{\theta}_{i,j}) &= \sum_{t=1}^n \log(\phi[\mathbf{S}_{ij}(t)]\phi[\mathbf{S}_{i'j'}(t)]\phi[\mathbf{I}_{2m-4}]) \\ &= \sum_{t=1}^n \log(f_1(i, j, t)) - (2m-4)n \log(2), \end{aligned} \quad (70)$$

and

$$\begin{aligned} \mathcal{L}(\tilde{\mathbf{Y}}; \boldsymbol{\theta} = \boldsymbol{\theta}_{i',j}) &= \sum_{t=1}^n \log(\phi[\mathbf{S}_{i'j}(t)]\phi[\mathbf{S}_{ij'}(t)]\phi[\mathbf{I}_{2m-4}]) \\ &= \sum_{t=1}^n \log(f_2(i, j, t)) - (2m-4)n \log(2), \end{aligned} \quad (71)$$

where $f_1(i, j, t)$ and $f_2(i, j, t)$ are

$$\begin{aligned} f_1(i, j, t) &= \phi[\mathbf{S}_{ij}(t)]\phi[\mathbf{S}_{i'j'}(t)] \\ &= \left(\frac{1}{4} + \frac{1}{2\pi} \arcsin[\tilde{y}_i(t)\tilde{y}_j(t)\rho_{ij}]\right) \\ &\quad \times \left(\frac{1}{4} + \frac{1}{2\pi} \arcsin[\tilde{y}_{i'}(t)\tilde{y}_{j'}(t)\rho_{i'j'}]\right) \\ &= \left(\frac{1}{4} + \frac{1}{2\pi} \tilde{y}_i(t)\tilde{y}_j(t) \arcsin \rho_{ij}\right) \\ &\quad \times \left(\frac{1}{4} + \frac{1}{2\pi} \tilde{y}_{i'}(t)\tilde{y}_{j'}(t) \arcsin \rho_{i'j'}\right), \end{aligned} \quad (72)$$

and

$$\begin{aligned} f_2(i, j, t) &= \phi[\mathbf{S}_{i'j}(t)]\phi[\mathbf{S}_{ij'}(t)] \\ &= \left(\frac{1}{4} + \frac{1}{2\pi} \arcsin[\tilde{y}_{i'}(t)\tilde{y}_j(t)\rho_{i'j}]\right) \\ &\quad \times \left(\frac{1}{4} + \frac{1}{2\pi} \arcsin[\tilde{y}_i(t)\tilde{y}_{j'}(t)\rho_{ij'}]\right) \\ &= \left(\frac{1}{4} + \frac{1}{2\pi} \tilde{y}_{i'}(t)\tilde{y}_j(t) \arcsin \rho_{i'j}\right) \\ &\quad \times \left(\frac{1}{4} + \frac{1}{2\pi} \tilde{y}_i(t)\tilde{y}_{j'}(t) \arcsin(-\rho_{ij'})\right). \end{aligned} \quad (73)$$

Using the definition of partial derivative, it is easy to show that

$$\begin{aligned} \left. \frac{\partial \mathcal{L}(\tilde{\mathbf{Y}}; \boldsymbol{\theta})}{\partial \rho_{ij}} \right|_{\boldsymbol{\theta}=\mathbf{0}} &= \lim_{\rho_{ij} \rightarrow 0} \frac{\mathcal{L}(\tilde{\mathbf{Y}}; \boldsymbol{\theta} = \boldsymbol{\theta}_{i,j}) - \mathcal{L}(\tilde{\mathbf{Y}}; \boldsymbol{\theta} = \mathbf{0})}{\rho_{ij}} \\ &= \frac{2}{\pi} \sum_{t=1}^n (\tilde{y}_i(t)\tilde{y}_j(t) + \tilde{y}_{i'}(t)\tilde{y}_{j'}(t)) \\ &= \frac{2n}{\pi} \text{Re}(\hat{r}_{ij}), \end{aligned} \quad (74)$$

and

$$\begin{aligned} \left. \frac{\partial \mathcal{L}(\tilde{\mathbf{Y}}; \boldsymbol{\theta})}{\partial \rho_{i'j}} \right|_{\boldsymbol{\theta}=\mathbf{0}} &= \lim_{\rho_{i'j} \rightarrow 0} \frac{\mathcal{L}(\tilde{\mathbf{Y}}; \boldsymbol{\theta} = \boldsymbol{\theta}_{i',j}) - \mathcal{L}(\tilde{\mathbf{Y}}; \boldsymbol{\theta} = \mathbf{0})}{\rho_{i'j}} \\ &= \frac{2}{\pi} \sum_{t=1}^n (\tilde{y}_{i'}(t)\tilde{y}_j(t) - \tilde{y}_i(t)\tilde{y}_{j'}(t)) \\ &= \frac{2n}{\pi} \text{Im}(\hat{r}_{ij}), \end{aligned} \quad (75)$$

where \hat{r}_{ij} is the (i, j) element of the SCM defined in (27), and we have used L'Hôpital's rule. Defining the vector $\hat{\mathbf{r}} \in \mathbb{C}^{(m^2-m)/2 \times 1}$ as

$$\hat{\mathbf{r}} = [\hat{r}_{1,2}, \hat{r}_{1,3}, \hat{r}_{2,3}, \dots, \hat{r}_{1,m}, \dots, \hat{r}_{m-1,m}]^T, \quad (76)$$

we combine (74) and (75) as

$$\left. \frac{\partial \mathcal{L}(\tilde{\mathbf{Y}}; \boldsymbol{\theta})}{\partial \boldsymbol{\theta}} \right|_{\boldsymbol{\theta}=\boldsymbol{\theta}_0} = \frac{2n}{\pi} \tilde{\mathbf{r}}, \quad (77)$$

where $\tilde{\mathbf{r}} = [\text{Re}(\hat{\mathbf{r}})^T, \text{Im}(\hat{\mathbf{r}})^T]^T$.

Plugging (77) into (25), the FIM can be rewritten as

$$\mathbf{F}(\boldsymbol{\theta}_0) = \frac{4n^2}{\pi^2} \mathbb{E}[\tilde{\mathbf{r}}\tilde{\mathbf{r}}^T]. \quad (78)$$

Under \mathcal{H}_0 , the PMF of $\tilde{\mathbf{Y}}$ is

$$p(\tilde{\mathbf{Y}}; \boldsymbol{\theta} = \boldsymbol{\theta}_0) = \left(\frac{1}{2}\right)^{2mn}, \quad (79)$$

allowing the computation of the expected values in (78). The expected value of the real parts is

$$\begin{aligned} \mathbb{E}[\text{Re}(\hat{r}_{ij})\text{Re}(\hat{r}_{kl})] &= \mathbb{E} \left[\frac{1}{n} \sum_{t=1}^n (\tilde{y}_i(t)\tilde{y}_j(t) + \tilde{y}_{i'}(t)\tilde{y}_{j'}(t)) \right. \\ &\quad \left. \times \frac{1}{n} \sum_{t=1}^n (\tilde{y}_k(t)\tilde{y}_l(t) + \tilde{y}_{k'}(t)\tilde{y}_{l'}(t)) \right] \\ &= \frac{2}{n} \delta_{ik} \delta_{jl}, \end{aligned} \quad (80)$$

and the expected value of the imaginary parts is

$$\begin{aligned} \mathbb{E}[\text{Im}(\hat{r}_{ij})\text{Im}(\hat{r}_{kl})] &= \mathbb{E} \left[\frac{1}{n} \sum_{t=1}^n (\tilde{y}_{i'}(t)\tilde{y}_j(t) - \tilde{y}_i(t)\tilde{y}_{j'}(t)) \right. \\ &\quad \left. \times \frac{1}{n} \sum_{t=1}^n (\tilde{y}_{k'}(t)\tilde{y}_l(t) - \tilde{y}_k(t)\tilde{y}_{l'}(t)) \right] \\ &= \frac{2}{n} \delta_{ik} \delta_{jl}, \end{aligned} \quad (81)$$

while the expected value of product between real and imaginary parts is

$$\begin{aligned} \mathbb{E}[\text{Re}(\hat{r}_{ij})\text{Im}(\hat{r}_{kl})] &= \mathbb{E} \left[\frac{1}{n} \sum_{t=1}^n (\tilde{y}_i(t)\tilde{y}_j(t) + \tilde{y}_{i'}(t)\tilde{y}_{j'}(t)) \right. \\ &\quad \left. \times \frac{1}{n} \sum_{t=1}^n (\tilde{y}_{k'}(t)\tilde{y}_l(t) - \tilde{y}_k(t)\tilde{y}_{l'}(t)) \right] \\ &= 0, \end{aligned} \quad (82)$$

where $1 \leq i < j \leq m$, $1 \leq k < l \leq m$, and δ_{ab} is the Kronecker delta function. Thus, we have

$$\mathbb{E}[\tilde{\mathbf{r}}\tilde{\mathbf{r}}^T] = \frac{2}{n} \mathbf{I}_{m^2-m}, \quad (83)$$

and (78) becomes

$$\mathbf{F}(\boldsymbol{\theta}_0) = \frac{8n}{\pi^2} \mathbf{I}_{m^2-m}. \quad (84)$$

Finally, by substituting (77) and (84) into (24), the proof is completed.

APPENDIX B PROOF OF THEOREM 2

Since the observations at different times are independent and $\tilde{y}_a(t)$ can only be $+1$ or -1 , we have

$$\mathbb{E} \left[\prod_{t=1}^n \prod_{a=1}^{2m} (\tilde{y}_a(t))^{\eta_{at}} \right] = \prod_{t=1}^n \mathbb{E} \left[\prod_{a=1}^{2m} (\tilde{y}_a(t))^{\text{mod}(\eta_{at}, 2)} \right], \quad (85)$$

where $\eta_{at} \in \mathbb{N}$ and $\text{mod}(\eta, 2)$ represents dividing η by 2 and obtaining the remainder. Using the PMF of $\tilde{\mathbf{Y}}$ under \mathcal{H}_0 in (79), we can easily get that the elements of $\tilde{\mathbf{Y}}$ are independent of each other and

$$\Pr\{\tilde{y}_a(t) = 1\} = \Pr\{\tilde{y}_a(t) = -1\} = \frac{1}{2}. \quad (86)$$

Therefore, under \mathcal{H}_0 , $\mathbb{E}\left[\prod_{t=1}^n \prod_{a=1}^{2m} (\tilde{y}_a(t))^{\eta_{at}}\right]$ can be calculated as

$$\begin{aligned} \mathbb{E}\left[\prod_{t=1}^n \prod_{a=1}^{2m} (\tilde{y}_a(t))^{\eta_{at}}\right] &= \prod_{t=1}^n \prod_{a=1}^{2m} \mathbb{E}\left[(\tilde{y}_a(t))^{\text{mod}(\eta_{at}, 2)}\right] \\ &= \begin{cases} 1, & \text{all } \eta_{at} \text{ are even,} \\ 0, & \text{otherwise,} \end{cases} \end{aligned} \quad (87)$$

Define $z_{ij}(t) = y_i(t)y_j^*(t)$. Using (87), we have

$$\mathbb{E}[z_{ij}(t_1)z_{ij}^*(t_2)] = 4\delta_{t_1 t_2}, \quad (88)$$

and

$$\begin{aligned} \mathbb{E}[z_{ij}(t_1)z_{ij}^*(t_2)z_{kl}(t_3)z_{kl}^*(t_4)] \\ = 16\delta_{t_1 t_2} \delta_{t_3 t_4} + 16\delta_{ik} \delta_{jl} \delta_{t_1 t_4} \delta_{t_2 t_3} (1 - \delta_{t_1 t_2} \delta_{t_3 t_4}), \end{aligned} \quad (89)$$

where $1 \leq i < j \leq m$, $1 \leq k < l \leq m$, $1 \leq t_1, t_2, t_3, t_4 \leq n$. Hence, under \mathcal{H}_0 , the mean of T_R^* is

$$\begin{aligned} \mu_0 &= \frac{1}{2m(m-1)} \sum_{\substack{i,j=1 \\ i < j}}^m \mathbb{E}\left[|\hat{r}_{ij}|^2\right] \\ &= \frac{1}{2m(m-1)} \sum_{\substack{i,j=1 \\ i < j}}^m \mathbb{E}\left[\frac{1}{n^2} \sum_{t_1, t_2=1}^n z_{ij}(t_1)z_{ij}^*(t_2)\right] \\ &= \frac{1}{n}, \end{aligned} \quad (90)$$

and its variance can be written as

$$\sigma_0^2 = \frac{1}{4m^2(m-1)^2} \left[\sum_{\substack{i,j,k,l=1 \\ i < j, k < l}}^m \mathbb{E}\left[|\hat{r}_{ij}|^2 |\hat{r}_{kl}|^2\right] \right] - \mu_0^2. \quad (91)$$

To compute (91), we need to obtain

$$\begin{aligned} \mathbb{E}\left[|\hat{r}_{ij}|^2 |\hat{r}_{kl}|^2\right] \\ = \mathbb{E}\left[\frac{1}{n^4} \sum_{t_1, t_2, t_3, t_4=1}^n z_{ij}(t_1)z_{ij}^*(t_2)z_{kl}(t_3)z_{kl}^*(t_4)\right] \\ = \frac{1}{n^4} \sum_{t_1, t_2, t_3, t_4=1}^n \mathbb{E}\left[z_{ij}(t_1)z_{ij}^*(t_2)z_{kl}(t_3)z_{kl}^*(t_4)\right] \\ = \frac{1}{n^4} [16n^2 + 16(n^2 - n)\delta_{ik}\delta_{jl}]. \end{aligned} \quad (92)$$

Substituting (90) and (92) into (91) yields

$$\begin{aligned} \sigma_0^2 &= \frac{1}{4m^2(m-1)^2 n^4} \sum_{\substack{i,j,k,l=1 \\ i < j, k < l}}^m [16n^2 + 16(n^2 - n)\delta_{ik}\delta_{jl}] - \frac{1}{n^2} \\ &= \frac{2(n-1)}{m(m-1)n^3} \end{aligned} \quad (93)$$

This completes the proof of Theorem 2.

APPENDIX C PROOF OF THEOREM 3

Under \mathcal{H}_1 , by combining the closed-form solution of the second and third-order center orthant probabilities in [62] and (21), we have the following expected values:

$$h_{ab} = \mathbb{E}[\tilde{y}_a(t)\tilde{y}_b(t)] = \frac{2}{\pi} \arcsin \rho_{ab}, \quad (94)$$

and

$$\begin{aligned} h_{abcd} &= \mathbb{E}[\tilde{y}_a(t)\tilde{y}_b(t)\tilde{y}_c(t)\tilde{y}_d(t)] \\ &= 16P_{abcd} - 1 - (h_{ab} + h_{ac} + h_{ad} + h_{bc} + h_{bd} + h_{cd}), \end{aligned} \quad (95)$$

where $1 \leq a \neq b \neq c \neq d \leq 2m$, and

$$P_{abcd} = \Pr\{\tilde{x}_a(t) > 0, \tilde{x}_b(t) > 0, \tilde{x}_c(t) > 0, \tilde{x}_d(t) > 0\}. \quad (96)$$

The probability P_{abcd} , which is the integral in the positive orthant of a 4-dimensional Gaussian distribution, can be computed using the results in [17]. Since $\rho_{ij} = \rho_{i'j'}$ and $\rho_{i'j} = -\rho_{ij'}$, where $1 \leq i < j \leq m$, we have

$$h_{i'j'} = h_{ij}, \quad h_{ij'} = -h_{i'j}. \quad (97)$$

Using (85), (94), (95), and (97), we can obtain the expected value of $z_{ij}(t)$:

$$\mathbb{E}[z_{ij}(t)] = 2(h_{ij} + ih_{i'j}), \quad (98)$$

and those of cross-products:

$$\begin{aligned} \mathbb{E}[z_{ij}(t)z_{kl}(t)] \\ = \begin{cases} 4h_{ii'jj'}, & i = k, j = l, \\ 2[h_{ii'j'l} + h_{ii'j'l} + \nu(h_{ii'jl} - h_{ii'j'l'})], & i = k, j \neq l, \\ 4(h_{kj} + ih_{k'j}), & i = l, \\ 4(h_{il} + ih_{i'l}), & j = k, \\ 2[h_{jj'ik'} + h_{jj'i'k} + \nu(h_{jj'i'k'} - h_{jj'ik})], & j = l, i \neq k, \\ \nu_1(i, j, k, l) - \nu_2(i, j, k, l) \\ + \nu[\nu_3(i, j, k, l) + \nu_4(i, j, k, l)], & i \neq j \neq k \neq l, \end{cases} \end{aligned} \quad (99)$$

and

$$\begin{aligned} \mathbb{E}[z_{ij}(t)z_{kl}^*(t)] \\ = \begin{cases} 4, & i = k, j = l, \\ 4(h_{ij} + \nu h_{i'j}), & i = k, j \neq l, \\ 2[h_{ii'jk'} + h_{ii'j'k} + \nu(h_{ii'jk} - h_{ii'j'k'})], & i = l, \\ 2[h_{jj'il} + h_{jj'i'l} + \nu(h_{jj'i'l'} - h_{jj'il})], & j = k, \\ 4(h_{ik} + \nu h_{i'k}), & j = l, i \neq k, \\ \nu_1(i, j, k, l) + \nu_2(i, j, k, l) \\ + \nu[\nu_3(i, j, k, l) - \nu_4(i, j, k, l)], & i \neq j \neq k \neq l, \end{cases} \end{aligned} \quad (100)$$

where $1 \leq i < j \leq m$, $1 \leq k < l \leq m$, $1 \leq t \leq n$,

$$\nu_1(i, j, k, l) = h_{ijkl} + h_{ijk'l'} + h_{i'j'kl} + h_{i'j'k'l'}, \quad (101a)$$

$$\nu_2(i, j, k, l) = h_{i'jk'l} - h_{i'jkl'} - h_{i'j'k'l} + h_{i'j'kl'}, \quad (101b)$$

$$\nu_3(i, j, k, l) = h_{i'jkl} + h_{i'jkl'} - h_{i'j'kl} - h_{i'j'k'l'}, \quad (101c)$$

$$\nu_4(i, j, k, l) = h_{ijk'l} - h_{ijk'l'} + h_{i'j'k'l} - h_{i'j'k'l'}. \quad (101d)$$

Therefore, the mean of T'_R under \mathcal{H}_1 is

$$\begin{aligned} \mu_1 &= \frac{1}{2m(m-1)} \sum_{\substack{i,j=1 \\ i < j}}^m \mathbb{E} [|\hat{r}_{ij}|^2] \\ &= \frac{1}{2m(m-1)} \sum_{\substack{i,j=1 \\ i < j}}^m \mathbb{E} \left[\frac{1}{n^2} \sum_{t=1}^n z_{ij}(t) z_{ij}^*(t) \right. \\ &\quad \left. + \frac{1}{n^2} \sum_{\substack{t_1, t_2=1 \\ t_1 \neq t_2}}^n z_{ij}(t_1) z_{ij}^*(t_2) \right] \\ &= \frac{1}{2m(m-1)} \sum_{\substack{i,j=1 \\ i < j}}^m g_{ij}, \end{aligned} \quad (102)$$

where

$$g_{ij} = \frac{4}{n^2} [n + A_{n,2} (h_{ij}^2 + h_{i'j'}^2)]. \quad (103)$$

Here, $A_{n,m} = \frac{n!}{m!}$ defines the number of permutations. In addition, the variance can be computed as

$$\begin{aligned} \sigma_1^2 &= \frac{1}{4m^2(m-1)^2} \left[\sum_{\substack{i,j,k,l=1 \\ i < j, k < l}}^m \mathbb{E} [|\hat{r}_{ij}|^2 |\hat{r}_{kl}|^2] \right. \\ &\quad \left. - \sum_{\substack{i,j,k,l=1 \\ i < j, k < l}}^m \mathbb{E} [|\hat{r}_{ij}|^2] \mathbb{E} [|\hat{r}_{kl}|^2] \right]. \end{aligned} \quad (104)$$

When $\delta_{t_1 t_2} + \delta_{t_3 t_4} \geq 1$, or $t_1 \neq t_2 \neq t_3 \neq t_4$, using (85), we have

$$\begin{aligned} &\mathbb{E}[z_{ij}(t_1) z_{ij}^*(t_2) z_{kl}(t_3) z_{kl}^*(t_4)] \\ &= \mathbb{E}[z_{ij}(t_1) z_{ij}^*(t_2)] \mathbb{E}[z_{kl}(t_3) z_{kl}^*(t_4)]. \end{aligned} \quad (105)$$

Then, the first term in (104) can be computed as:

$$\begin{aligned} &\mathbb{E} [|\hat{r}_{ij}|^2 |\hat{r}_{kl}|^2] \\ &= \frac{1}{n^4} \mathbb{E} \left[\sum_{t_1, t_2, t_3, t_4=1}^n z_{ij}(t_1) z_{ij}^*(t_2) z_{kl}(t_3) z_{kl}^*(t_4) \right] \\ &= \mathbb{E} [|\hat{r}_{ij}|^2] \mathbb{E} [|\hat{r}_{kl}|^2] \\ &\quad + \frac{1}{n^4} \sum_{\substack{t_1, t_2, t_3, t_4=1 \\ (t_1, t_2, t_3, t_4) \in \mathbb{T}}}^n \mathbb{E} [z_{ij}(t_1) z_{ij}^*(t_2) z_{kl}(t_3) z_{kl}^*(t_4)] \\ &\quad - \frac{1}{n^4} \sum_{\substack{t_1, t_2, t_3, t_4=1 \\ (t_1, t_2, t_3, t_4) \in \mathbb{T}}}^n \mathbb{E} [z_{ij}(t_1) z_{ij}^*(t_2)] \mathbb{E} [z_{kl}(t_3) z_{kl}^*(t_4)], \end{aligned} \quad (106)$$

where

$$\mathbb{T} = \{(a, b, c, d) | \delta_{ab} + \delta_{cd} = 0, \delta_{ac} + \delta_{ad} + \delta_{bc} + \delta_{bd} \geq 1\}. \quad (107)$$

Taking into account (98), (99), and (100), it can be shown that

$$\mathbb{E} [|\hat{r}_{ij}|^2 |\hat{r}_{kl}|^2] = \mathbb{E} [|\hat{r}_{ij}|^2] \mathbb{E} [|\hat{r}_{kl}|^2] + f_{ijkl} - g_{ijkl}, \quad (108)$$

where

$$g_{ijkl} = \frac{32(n-1)(2n-3)}{n^3} (h_{ij}^2 + h_{i'j'}^2)(h_{kl}^2 + h_{k'l'}^2). \quad (109)$$

and

$$f_{ijkl} = \begin{cases} \tau_1(i, j), & i = k, j = l, \\ \tau_2(i, j, l), & i = k, j \neq l, \\ \tau_2(i, j, k), & i = l, \\ \tau_2(j, i, l), & j = k, \\ \tau_2(j, i, k), & j = l, i \neq k, \\ \tau_3(j, i, k, l), & i \neq j \neq k \neq l, \end{cases} \quad (110)$$

with

$$\begin{aligned} \tau_1(i, j) &= \frac{16}{n^4} A_{n,2} [1 + h_{ii'jj'}^2] \\ &\quad + \frac{32}{n^4} A_{n,3} [(h_{ij}^2 + h_{i'j'}^2) + h_{ii'jj'}(h_{ij}^2 - h_{i'j'}^2)], \end{aligned} \quad (111)$$

$$\begin{aligned} \tau_2(i, j, k) &= \frac{4}{n^4} A_{n,2} [4(h_{jk}^2 + h_{j'k'}^2) + (h_{ii'jk'} + h_{ii'j'k})^2 \\ &\quad + (h_{ii'jk} - h_{ii'j'k'})^2] \\ &\quad + \frac{16}{n^4} A_{n,3} [(h_{ii'jk} - h_{ii'j'k'}) (h_{ik} h_{i'j} + h_{ij} h_{i'k}) \\ &\quad + (h_{ii'jk'} + h_{ii'j'k'}) (h_{ik} h_{ij} - h_{i'j} h_{i'k}) \\ &\quad + 2h_{jk} (h_{ik} h_{ij} + h_{i'j} h_{i'k}) \\ &\quad + 2h_{j'k'} (h_{ik} h_{i'j} - h_{ij} h_{i'k})], \end{aligned} \quad (112)$$

and

$$\begin{aligned} \tau_3(i, j, k, l) &= \frac{2}{n^4} A_{n,2} \sum_{t=1}^4 v_t^2(i, j, k, l) \\ &\quad + \frac{16}{n^4} A_{n,3} [v_1(i, j, k, l) h_{ij} h_{kl} \\ &\quad + v_2(i, j, k, l) h_{i'j} h_{k'l} \\ &\quad + v_3(i, j, k, l) h_{kl} h_{i'j} \\ &\quad + v_4(i, j, k, l) h_{ij} h_{k'l}]. \end{aligned} \quad (113)$$

Hence, the variance of T'_R under \mathcal{H}_1 is

$$\sigma_1^2 = \frac{1}{4m^2(m-1)^2} \sum_{\substack{i,j,k,l=1 \\ i < j, k < l}}^m (f_{ijkl} - g_{ijkl}), \quad (115)$$

which completes the proof of Theorem 3.

APPENDIX D MEAN AND COVARIANCE MATRIX OF $\tilde{\mathbf{r}}_{sc}$

We derive the mean and covariance matrix of $\tilde{\mathbf{r}}_{sc}$ and postpone the proof of Gaussianity to Appendix E.

For convenience, we define a random vector \mathbf{r} with the subscript sc to mean scaling as follows:

$$\mathbf{r}_{sc} = \sqrt{\frac{n}{2}} \mathbf{r}. \quad (116)$$

Then, $\tilde{\mathbf{r}}_{\text{sc}}$ can be rewritten as $\tilde{\mathbf{r}}_{\text{sc}} = [\text{Re}(\hat{\mathbf{r}}_{\text{sc}})^T, \text{Im}(\hat{\mathbf{r}}_{\text{sc}})^T]^T$, where

$$\hat{\mathbf{r}}_{\text{sc}} = [(\hat{r}_{1,2})_{\text{sc}}, (\hat{r}_{1,3})_{\text{sc}}, (\hat{r}_{2,3})_{\text{sc}}, \dots, (\hat{r}_{1,m})_{\text{sc}}, \dots, (\hat{r}_{m-1,m})_{\text{sc}}]^T. \quad (117)$$

Since $\boldsymbol{\theta}$ is assumed of order $\mathcal{O}(n^{-\frac{1}{2}})$, we can apply a Taylor's approximation to $p(\tilde{\mathbf{y}}(t); \boldsymbol{\theta})$ around $\boldsymbol{\theta}_0 = \mathbf{0}$, allowing us to write

$$\begin{aligned} p(\tilde{\mathbf{y}}(t); \boldsymbol{\theta}) &= p(\tilde{\mathbf{y}}(t); \boldsymbol{\theta}_0) + \boldsymbol{\theta}^T \frac{\partial p(\tilde{\mathbf{y}}(t))}{\partial \boldsymbol{\theta}} \Big|_{\boldsymbol{\theta}=\boldsymbol{\theta}_0} + \mathcal{O}(n^{-1}) \\ &= \frac{1}{2^{2m}} + \frac{1}{2^{2m-1}\pi} \sum_{\substack{i,j=1 \\ i < j}}^m \text{Re}(z_{ij}(t)) \rho_{ij} \\ &\quad + \frac{1}{2^{2m-1}\pi} \sum_{\substack{i,j=1 \\ i < j}}^m \text{Im}(z_{ij}(t)) \rho_{i'j} + \mathcal{O}(n^{-1}), \end{aligned} \quad (118)$$

where the elements of $\frac{\partial p(\tilde{\mathbf{y}}(t))}{\partial \boldsymbol{\theta}} \Big|_{\boldsymbol{\theta}=\boldsymbol{\theta}_0}$ are obtained similarly to (74) and (75). Since $\rho_{i'j'} = \rho_{ij}$, $\rho_{ij'} = -\rho_{i'j}$ and $\text{diag}(\text{Im}(\mathbf{P}_{\mathbf{x}})) = \mathbf{0}$, $p(\tilde{\mathbf{y}}(t); \boldsymbol{\theta})$ can be rewritten as

$$p(\tilde{\mathbf{y}}(t); \boldsymbol{\theta}) = \frac{1}{2^{2m}} + \frac{1}{2^{2m-1}\pi} \sum_{\substack{i,j=1 \\ i < j}}^{2m} \tilde{y}_i(t) \tilde{y}_j(t) \rho_{ij} + \mathcal{O}(n^{-1}). \quad (119)$$

From this PMF, it is easy to obtain

$$p(\tilde{y}_a(t), \tilde{y}_b(t); \boldsymbol{\theta}) = \frac{1}{4} + \frac{1}{2\pi} \tilde{y}_a(t) \tilde{y}_b(t) \rho_{ab} + \mathcal{O}(n^{-1}), \quad (120)$$

and

$$\begin{aligned} p(\tilde{y}_a(t), \tilde{y}_b(t), \tilde{y}_c(t), \tilde{y}_d(t); \boldsymbol{\theta}) &= \frac{1}{16} + \frac{1}{8\pi} \tilde{y}_a(t) \tilde{y}_b(t) \rho_{ab} + \frac{1}{8\pi} \tilde{y}_a(t) \tilde{y}_c(t) \rho_{ac} \\ &\quad + \frac{1}{8\pi} \tilde{y}_a(t) \tilde{y}_d(t) \rho_{ad} + \frac{1}{8\pi} \tilde{y}_b(t) \tilde{y}_c(t) \rho_{bc} \\ &\quad + \frac{1}{8\pi} \tilde{y}_b(t) \tilde{y}_d(t) \rho_{bd} + \frac{1}{8\pi} \tilde{y}_c(t) \tilde{y}_d(t) \rho_{cd} \\ &\quad + \mathcal{O}(n^{-1}), \end{aligned} \quad (121)$$

where $1 \leq a \neq b \neq c \neq d \leq 2m$. As a consequence, we have

$$\begin{aligned} \mathbb{E}[\tilde{y}_a(t) \tilde{y}_b(t)] &= \sum_{\substack{\tilde{y}_e(t)=\pm 1 \\ e=a,b}} \tilde{y}_a(t) \tilde{y}_b(t) p(\tilde{y}_a(t), \tilde{y}_b(t); \boldsymbol{\theta}) \\ &= \frac{2}{\pi} \rho_{ab} + \mathcal{O}(n^{-1}), \end{aligned} \quad (122)$$

and

$$\begin{aligned} \mathbb{E}[\tilde{y}_a(t) \tilde{y}_b(t) \tilde{y}_c(t) \tilde{y}_d(t)] &= \sum_{\substack{\tilde{y}_e(t)=\pm 1 \\ e=a,b,c,d}} \tilde{y}_a(t) \tilde{y}_b(t) \tilde{y}_c(t) \tilde{y}_d(t) p(\tilde{y}_a(t), \tilde{y}_b(t), \tilde{y}_c(t), \tilde{y}_d(t); \boldsymbol{\theta}) \\ &= \mathcal{O}(n^{-1}). \end{aligned} \quad (123)$$

When some or all of the indexes $\{a, b, c, d\}$ are identical, $\mathbb{E}[\tilde{y}_a(t) \tilde{y}_b(t) \tilde{y}_c(t) \tilde{y}_d(t)]$ can be simplified by (85). Thus, we can show

$$\begin{aligned} \mathbb{E}[\text{Re}((\hat{r}_{ij})_{\text{sc}})] &= \sqrt{\frac{n}{2}} \mathbb{E}[\text{Re}(\hat{r}_{ij})] \\ &= \sqrt{\frac{n}{2}} \mathbb{E} \left[\frac{1}{n} \sum_{t=1}^n (\tilde{y}_i(t) \tilde{y}_j(t) + \tilde{y}_{i'}(t) \tilde{y}_{j'}(t)) \right] \\ &= \sqrt{\frac{n}{2}} \left[\frac{2}{\pi} \rho_{ij} + \frac{2}{\pi} \rho_{i'j'} + \mathcal{O}(n^{-1}) \right] \\ &= \frac{2\sqrt{2n}}{\pi} \rho_{ij} + \mathcal{O}(n^{-\frac{1}{2}}), \end{aligned} \quad (124)$$

and

$$\begin{aligned} \mathbb{E}[\text{Im}((\hat{r}_{ij})_{\text{sc}})] &= \sqrt{\frac{n}{2}} \mathbb{E}[\text{Im}(\hat{r}_{ij})] \\ &= \sqrt{\frac{n}{2}} \mathbb{E} \left[\frac{1}{n} \sum_{t=1}^n (\tilde{y}_{i'}(t) \tilde{y}_j(t) - \tilde{y}_i(t) \tilde{y}_{j'}(t)) \right] \\ &= \sqrt{\frac{n}{2}} \left[\frac{2}{\pi} \rho_{i'j} - \frac{2}{\pi} \rho_{ij'} + \mathcal{O}(n^{-1}) \right] \\ &= \frac{2\sqrt{2n}}{\pi} \rho_{i'j} + \mathcal{O}(n^{-\frac{1}{2}}), \end{aligned} \quad (125)$$

and the expected value of $\tilde{\mathbf{r}}$ becomes

$$\mathbb{E}[\tilde{\mathbf{r}}_{\text{sc}}] = \frac{2\sqrt{2n}}{\pi} \boldsymbol{\theta} + \mathcal{O}(n^{-\frac{1}{2}}). \quad (126)$$

Since the observations at different times are independent, for $t_1 \neq t_2$, we have

$$\mathbb{E}[\tilde{y}_a(t_1) \tilde{y}_b(t_1) \tilde{y}_c(t_2) \tilde{y}_d(t_2)] = \mathbb{E}[\tilde{y}_a(t_1) \tilde{y}_b(t_1)] \mathbb{E}[\tilde{y}_c(t_2) \tilde{y}_d(t_2)]. \quad (127)$$

To proceed, we need to compute

$$\begin{aligned} \mathbb{E}[\text{Re}((\hat{r}_{ij})_{\text{sc}}) \text{Re}((\hat{r}_{kl})_{\text{sc}})] &- \mathbb{E}[\text{Re}((\hat{r}_{ij})_{\text{sc}})] \mathbb{E}[\text{Re}((\hat{r}_{kl})_{\text{sc}})] \\ &= \frac{n}{2} \mathbb{E}[\text{Re}(\hat{r}_{ij}) \text{Re}(\hat{r}_{kl})] - \frac{n}{2} \mathbb{E}[\text{Re}(\hat{r}_{ij})] \mathbb{E}[\text{Re}(\hat{r}_{kl})] \\ &= \frac{1}{2n} \mathbb{E} \left[\sum_{t_1, t_2=1}^n \text{Re}(z_{ij}(t_1)) \text{Re}(z_{kl}(t_2)) \right] \\ &\quad - \frac{1}{2n} \mathbb{E} \left[\sum_{t_1=1}^n \text{Re}(z_{ij}(t_1)) \right] \mathbb{E} \left[\sum_{t_2=1}^n \text{Re}(z_{kl}(t_2)) \right] \\ &= \frac{1}{2n} \sum_{t=1}^n \mathbb{E} [\text{Re}(z_{ij}(t)) \text{Re}(z_{kl}(t))] \\ &\quad - \frac{1}{2n} \sum_{t=1}^n \mathbb{E} [\text{Re}(z_{ij}(t))] \mathbb{E} [\text{Re}(z_{kl}(t))] \\ &= \begin{cases} \left(1 - \frac{8}{\pi^2} \rho_{ij}^2 + \mathcal{O}(n^{-1}), & i = k, j = l, \right. \\ \frac{2}{\pi} \rho_{jl} - \frac{8}{\pi^2} \rho_{ij} \rho_{il} + \mathcal{O}(n^{-1}), & i = k, j \neq l, \\ \frac{2}{\pi} \rho_{jk} - \frac{8}{\pi^2} \rho_{ij} \rho_{ki} + \mathcal{O}(n^{-1}), & i = l, \\ \frac{2}{\pi} \rho_{il} - \frac{8}{\pi^2} \rho_{ij} \rho_{jl} + \mathcal{O}(n^{-1}), & j = k, \\ \frac{2}{\pi} \rho_{ik} - \frac{8}{\pi^2} \rho_{ij} \rho_{kj} + \mathcal{O}(n^{-1}), & j = l, i \neq k, \\ \left. - \frac{8}{\pi^2} \rho_{ij} \rho_{kl} + \mathcal{O}(n^{-1}), & i \neq j \neq k \neq l. \right. \end{cases} \end{aligned} \quad (128)$$

Since $\boldsymbol{\theta}$ is of order $\mathcal{O}(n^{-\frac{1}{2}})$, the result of (128) can be rewritten as

$$\begin{aligned} & \mathbb{E}[\text{Re}((\hat{r}_{ij})_{\text{sc}}) \text{Re}((\hat{r}_{kl})_{\text{sc}})] - \mathbb{E}[\text{Re}((\hat{r}_{ij})_{\text{sc}})]\mathbb{E}[\text{Re}((\hat{r}_{kl})_{\text{sc}})] \\ &= \begin{cases} 1 + \mathcal{O}(n^{-1}), & i = k, j = l, \\ \mathcal{O}(n^{-\frac{1}{2}}), & \text{otherwise,} \end{cases} \end{aligned} \quad (129)$$

where $1 \leq i < j \leq m$ and $1 \leq k < l \leq m$. Similarly, we have

$$\begin{aligned} & \mathbb{E}[\text{Re}((\hat{r}_{ij})_{\text{sc}}) \text{Im}((\hat{r}_{kl})_{\text{sc}})] - \mathbb{E}[\text{Re}((\hat{r}_{ij})_{\text{sc}})]\mathbb{E}[\text{Im}((\hat{r}_{kl})_{\text{sc}})] \\ &= \mathcal{O}(n^{-\frac{1}{2}}), \end{aligned} \quad (130)$$

and

$$\begin{aligned} & \mathbb{E}[\text{Im}((\hat{r}_{ij})_{\text{sc}}) \text{Im}((\hat{r}_{kl})_{\text{sc}})] - \mathbb{E}[\text{Im}((\hat{r}_{ij})_{\text{sc}})]\mathbb{E}[\text{Im}((\hat{r}_{kl})_{\text{sc}})] \\ &= \begin{cases} 1 + \mathcal{O}(n^{-1}), & i = k, j = l, \\ \mathcal{O}(n^{-\frac{1}{2}}), & \text{otherwise,} \end{cases} \end{aligned} \quad (131)$$

Hence, the covariance matrix of $\tilde{\mathbf{r}}_{\text{sc}}$ for low SNR is

$$\mathbf{R}_{\tilde{\mathbf{r}}_{\text{sc}}} = \mathbf{I}_{m^2-m} + \mathcal{O}(n^{-\frac{1}{2}}). \quad (132)$$

APPENDIX E PROOF OF GAUSSIANTY OF $\tilde{\mathbf{r}}_{\text{sc}}$

We prove that $\tilde{\mathbf{r}}_{\text{sc}}$ asymptotically follows a Gaussian distribution, which completes the proof of Theorem 4. For this proof, we need the following lemma, which is a multivariate version of the central limit theorem [63].

Lemma 1: Let $\mathbf{s} = \sum_{t=1}^n \mathbf{b}_t$, where $\mathbf{b}_1, \dots, \mathbf{b}_n \in \mathbb{R}^{d \times 1}$ are mutually independent random vectors with zero mean. Then, as $n \rightarrow \infty$, \mathbf{s} is asymptotically Gaussian distributed with zero mean and covariance matrix \mathbf{C} if

$$\lim_{n \rightarrow \infty} \sum_{t=1}^n \mathbb{E} \left[\left\| \mathbf{C}^{-1/2} \mathbf{b}_t \right\|^3 \right] = 0. \quad (133)$$

To use Lemma 1, we first define a new set of variables

$$\tilde{\mathbf{z}}_t = \sqrt{\frac{1}{2n}} [\text{Re}(\mathbf{z}_t)^T, \text{Im}(\mathbf{z}_t)^T]^T, \quad (134)$$

where $1 \leq i \leq n$, and

$$\mathbf{z}_t = [z_{1,2}(t), z_{1,3}(t), \dots, z_{m-1,m}(t)]^T. \quad (135)$$

We also define

$$\mathbf{b}_t = \tilde{\mathbf{z}}_t - \mathbb{E}[\tilde{\mathbf{z}}_t]. \quad (136)$$

Using (98), we have

$$\mathbb{E}[\tilde{\mathbf{z}}_t] = \left(\frac{8}{n\pi^2} \right)^{\frac{1}{2}} \arcsin \boldsymbol{\theta}, \quad (137)$$

where arcsin applying to its argument in an element-wise manner. We also define

$$\mathbf{s} = \sum_{t=1}^n \mathbf{b}_t, \quad (138)$$

as in the previous lemma, which allows us to write $\tilde{\mathbf{r}}_{\text{sc}}$ in Theorem 4 as

$$\tilde{\mathbf{r}}_{\text{sc}} = \mathbf{s} + \mathbb{E}[\tilde{\mathbf{r}}_{\text{sc}}], \quad (139)$$

where the mean of $\tilde{\mathbf{r}}_{\text{sc}}$ is given by

$$\mathbb{E}[\tilde{\mathbf{r}}_{\text{sc}}] = \sum_{t=1}^n \mathbb{E}[\tilde{\mathbf{z}}_t] = \left(\frac{8n}{\pi^2} \right)^{\frac{1}{2}} \arcsin \boldsymbol{\theta}. \quad (140)$$

In addition, \mathbf{C} is equal to $\mathbf{R}_{\tilde{\mathbf{r}}_{\text{sc}}}$ which is the covariance matrix of $\tilde{\mathbf{r}}_{\text{sc}}$.

Since translation does not change the distribution type of the variables, we only need to prove that \mathbf{s} is asymptotically Gaussian distributed to complete the proof of Theorem 4.

Defining \mathbf{c}_i as the i th row vector of $\mathbf{C}^{-1/2}$, we have

$$\left\| \mathbf{C}^{-1/2} \mathbf{b}_t \right\|^3 = \left(\left\| \mathbf{C}^{-1/2} \mathbf{b}_t \right\|^2 \right)^{\frac{3}{2}} = \left(\sum_{i=1}^{m(m-1)} \|\mathbf{c}_i \mathbf{b}_t\|^2 \right)^{\frac{3}{2}}. \quad (141)$$

The Cauchy-Schwarz inequality allows us to write

$$\|\mathbf{c}_i \mathbf{b}_t\|^2 \leq \|\mathbf{c}_i\|^2 \|\mathbf{b}_t\|^2, \quad (142)$$

which yields

$$\begin{aligned} \left\| \mathbf{C}^{-1/2} \mathbf{b}_t \right\|^3 &\leq \left(\sum_{i=1}^{m(m-1)} \|\mathbf{c}_i\|^2 \|\mathbf{b}_t\|^2 \right)^{\frac{3}{2}} \\ &= \left(\left\| \mathbf{C}^{-1/2} \right\|^2 \|\mathbf{b}_t\|^2 \right)^{\frac{3}{2}} \\ &= \left\| \mathbf{C}^{-1/2} \right\|^3 \|\mathbf{b}_t\|^3 \end{aligned} \quad (143)$$

Using the inequality $\mathbb{E}[f(x)] \geq \mathbb{E}[g(x)]$, for $f(x) \geq g(x) \geq 0$, we have

$$\mathbb{E} \left[\left\| \mathbf{C}^{-1/2} \mathbf{b}_t \right\|^3 \right] \leq \left\| \mathbf{C}^{-1/2} \right\|^3 \mathbb{E} \left[\|\mathbf{b}_t\|^3 \right], \quad (144)$$

Since $\left\| \mathbf{C}^{-1/2} \right\|^3$ is bounded and using the previous inequality, a sufficient condition for (133) is

$$\lim_{n \rightarrow \infty} \sum_{t=1}^n \mathbb{E} \left[\|\mathbf{b}_t\|^3 \right] = 0. \quad (145)$$

Using (136) and the parallelogram law [64], we have

$$\|\mathbf{b}_t\|^2 + \|\tilde{\mathbf{z}}_t + \mathbb{E}[\tilde{\mathbf{z}}_t]\|^2 = 2 \left(\|\tilde{\mathbf{z}}_t\|^2 + \|\mathbb{E}[\tilde{\mathbf{z}}_t]\|^2 \right). \quad (146)$$

Since that $\|\tilde{\mathbf{z}}_t + \mathbb{E}[\tilde{\mathbf{z}}_t]\|^2 \geq 0$, we have

$$\|\mathbf{b}_t\|^2 \leq 2 \left(\|\tilde{\mathbf{z}}_t\|^2 + \|\mathbb{E}[\tilde{\mathbf{z}}_t]\|^2 \right). \quad (147)$$

Therefore,

$$\begin{aligned} \max \|\mathbf{b}_t\|^2 &\leq \max 2 \left(\|\tilde{\mathbf{z}}_t\|^2 + \|\mathbb{E}[\tilde{\mathbf{z}}_t]\|^2 \right) \\ &= \max 2 \left(\frac{m(m-1)}{n} + \frac{8}{n\pi^2} \|\arcsin \boldsymbol{\theta}\|^2 \right) \\ &= \frac{2m(m-1)}{n} + \frac{16}{n\pi^2} \max_{\boldsymbol{\theta}} \|\arcsin \boldsymbol{\theta}\|^2 \\ &= \frac{6m(m-1)}{n}. \end{aligned} \quad (148)$$

Thus, it can be shown that

$$\begin{aligned}
 \lim_{n \rightarrow \infty} \sum_{t=1}^n \mathbb{E} \left[\|\mathbf{b}_t\|^3 \right] &\leq \lim_{n \rightarrow \infty} \sum_{t=1}^n \max \left[\|\mathbf{b}_t\|^3 \right] \\
 &= \lim_{n \rightarrow \infty} \sum_{t=1}^n \left[\left(\max \|\mathbf{b}_t\|^2 \right)^{\frac{3}{2}} \right] \\
 &\leq [6m(m-1)]^{\frac{3}{2}} \lim_{n \rightarrow \infty} n^{-\frac{1}{2}} \\
 &= 0.
 \end{aligned} \tag{149}$$

This completes the proof.

ACKNOWLEDGMENT

The authors acknowledge the assistance of OpenAI's language model, ChatGPT, in proofreading and enhancing the clarity of this manuscript. However, it is important to note that the generation of technical content lies solely with the authors.

REFERENCES

- [1] C. Sun, W. Zhang, and K. B. Letaief, "Cooperative spectrum sensing for cognitive radios under bandwidth constraints," in *Proc. IEEE Wireless Commun. Netw. Conf. (WCNC)*, Hong Kong, China, Mar. 2007, pp. 1–5.
- [2] J. Ma, G. Zhao, and Y. Li, "Soft combination and detection for cooperative spectrum sensing in cognitive radio networks," *IEEE Trans. Wireless Commun.*, vol. 7, no. 11, pp. 4502–4507, Nov. 2008.
- [3] L. Wei and O. Tirkkonen, "Spectrum sensing in the presence of multiple primary users," *IEEE Trans. Commun.*, vol. 60, no. 5, pp. 1268–1277, May 2012.
- [4] L. Wei, P. Dharmawansa, and O. Tirkkonen, "Multiple primary user spectrum sensing in the low SNR regime," *IEEE Trans. Commun.*, vol. 61, no. 5, pp. 1720–1731, May 2013.
- [5] L. Huang, Y.-H. Xiao, and Q. T. Zhang, "Robust spectrum sensing for noncircular signal in multiantenna cognitive receivers," *IEEE Trans. Signal Process.*, vol. 63, no. 2, pp. 498–511, Jan. 2015.
- [6] J. Choi, J. Mo, and R. W. Heath, "Near maximum-likelihood detector and channel estimator for uplink multiuser massive MIMO systems with one-bit ADCs," *IEEE Trans. Commun.*, vol. 64, no. 5, pp. 2005–2018, May 2016.
- [7] R. H. Walden, "Analog-to-digital converter survey and analysis," *IEEE J. Sel. Areas Commun.*, vol. 17, no. 4, pp. 539–550, Apr. 1999.
- [8] B. Murmann, "The race for the extra decibel: A brief review of current ADC performance trajectories," *IEEE Solid-State Circuits Mag.*, vol. 7, no. 3, pp. 58–66, Sep. 2015.
- [9] A. Ali and W. Hamouda, "Generalized FFT-based one-bit quantization system for wideband spectrum sensing," *IEEE Trans. Commun.*, vol. 68, no. 1, pp. 82–92, Jan. 2020.
- [10] B. T. Reyes, L. Biolato, A. C. Galetto, L. Passetti, F. Solis, and M. R. Hueda, "An energy-efficient hierarchical architecture for time-interleaved SAR ADC," *IEEE Trans. Circuits Syst. I, Reg. Papers*, vol. 66, no. 6, pp. 2064–2076, Jun. 2019.
- [11] V. R. Bhumireddy et al., "Design of low power and high speed comparator with sub-32-nm Double Gate-MOSFET," in *Proc. ICCAS IEEE Int. Conf. Circuits Syst. (ICCAS)*, Kuala Lumpur, Malaysia, Sep. 2013, pp. 1–4.
- [12] Y.-H. Xiao, D. Ramírez, P. J. Schreier, C. Qian, and L. Huang, "One-bit target detection in collocated MIMO radar and performance degradation analysis," *IEEE Trans. Veh. Technol.*, vol. 71, no. 9, pp. 9363–9374, Sep. 2022.
- [13] A. Ali and W. Hamouda, "Low power wideband sensing for one-bit quantized cognitive radio systems," *IEEE Wireless Commun. Lett.*, vol. 5, no. 1, pp. 16–19, Feb. 2016.
- [14] Z. Cheng, Z. He, and B. Liao, "Target detection performance of collocated MIMO radar with one-bit ADCs," *IEEE Signal Process. Lett.*, vol. 26, no. 12, pp. 1832–1836, Dec. 2019.
- [15] D. Ciuonzo, G. Papa, G. Romano, P. S. Rossi, and P. Willett, "One-bit decentralized detection with a Rao test for multisensor fusion," *IEEE Signal Process. Lett.*, vol. 20, no. 9, pp. 861–864, Sep. 2013.
- [16] O. Bar-Shalom and A. J. Weiss, "DOA estimation using one-bit quantized measurements," *IEEE Trans. Aerosp. Electron. Syst.*, vol. 38, no. 3, pp. 868–884, Jul. 2002.
- [17] I. G. Abrahamson, "Orthant probabilities for the quadrivariate normal distribution," *Ann. Math. Statist.*, vol. 35, no. 4, pp. 1685–1703, Dec. 1964.
- [18] P. Craig, "A new reconstruction of multivariate normal orthant probabilities," *J. Roy. Statist. Soc. Ser. B-Statist. Methodol.*, vol. 70, no. 1, pp. 227–243, Feb. 2008.
- [19] J. Fang, Y. Liu, H. Li, and S. Li, "One-bit quantizer design for multisensor GLRT fusion," *IEEE Signal Process. Lett.*, vol. 20, no. 3, pp. 257–260, Mar. 2013.
- [20] T. Yucek and H. Arslan, "A survey of spectrum sensing algorithms for cognitive radio applications," *IEEE Commun. Surveys Tuts.*, vol. 11, no. 1, pp. 116–130, Mar. 2009.
- [21] L. Huang, J. Fang, K. Liu, H. C. So, and H. Li, "An eigenvalue-moment-ratio approach to blind spectrum sensing for cognitive radio under sample-starving environment," *IEEE Trans. Veh. Technol.*, vol. 64, no. 8, pp. 3465–3480, Aug. 2015.
- [22] Y. Zhao, X. Ke, B. Zhao, Y. Xiao, and L. Huang, "One-bit spectrum sensing based on statistical covariances: Eigenvalue moment ratio approach," *IEEE Wireless Commun. Lett.*, vol. 10, no. 11, pp. 2474–2478, Nov. 2021.
- [23] J. H. Van Vleck and D. Middleton, "The spectrum of clipped noise," *Proc. IEEE*, vol. 54, no. 1, pp. 2–19, Jan. 1966.
- [24] A. Høst-Madsen and P. Handel, "Effects of sampling and quantization on single-tone frequency estimation," *IEEE Trans. Signal Process.*, vol. 48, no. 3, pp. 650–662, Mar. 2000.
- [25] A. Mezghani and J. A. Nossek, "On ultra-wideband MIMO systems with 1-bit quantized outputs: Performance analysis and input optimization," in *Proc. IEEE Int. Symp. Inf. Theory*, Nice, France, Jun. 2007, pp. 1286–1289.
- [26] A. J. Viterbi and J. K. Omura, *Principles of Digital Communication and Coding*. New York, NY, USA: Dover, 2013.
- [27] M. S. Stein, S. Bar, J. A. Nossek, and J. Tabrikian, "Performance analysis for channel estimation with 1-bit ADC and unknown quantization threshold," *IEEE Trans. Signal Process.*, vol. 66, no. 10, pp. 2557–2571, May 2018.
- [28] H. C. Papadopoulos, G. W. Wornell, and A. V. Oppenheim, "Sequential signal encoding from noisy measurements using quantizers with dynamic bias control," *IEEE Trans. Inf. Theory*, vol. 47, no. 3, pp. 978–1002, Mar. 2001.
- [29] A. Mezghani, J. A. Nossek, and A. L. Swindlehurst, "Low SNR asymptotic rates of vector channels with one-bit outputs," *IEEE Trans. Inf. Theory*, vol. 66, no. 12, pp. 7615–7634, Dec. 2020.
- [30] Y.-H. Xiao, L. Huang, J. Xie, and H. C. So, "Approximate asymptotic distribution of locally most powerful invariant test for independence: Complex case," *IEEE Trans. Inf. Theory*, vol. 64, no. 3, pp. 1784–1799, Mar. 2018.
- [31] L. Huang, Y. Xiao, H. C. So, and J. Fang, "Accurate performance analysis of Hadamard ratio test for robust spectrum sensing," *IEEE Trans. Wireless Commun.*, vol. 14, no. 2, pp. 750–758, Feb. 2015.
- [32] S. John, "Some optimal multivariate tests," *Biometrika*, vol. 58, no. 1, pp. 123–127, Apr. 1971.
- [33] D. Ramírez, J. Via, I. Santamaría, and L. L. Scharf, "Locally most powerful invariant tests for correlation and sphericity of Gaussian vectors," *IEEE Trans. Inf. Theory*, vol. 59, no. 4, pp. 2128–2141, Apr. 2013.
- [34] D. Ramírez, G. Vazquez-Vilar, R. Lopez-Valcarce, J. Via, and I. Santamaría, "Detection of rank- P signals in cognitive radio networks with uncalibrated multiple antennas," *IEEE Trans. Signal Process.*, vol. 59, no. 8, pp. 3764–3774, Aug. 2011.
- [35] A. Leshem and A.-J. van der Veen, "Multichannel detection of Gaussian signals with uncalibrated receivers," *IEEE Signal Process. Lett.*, vol. 8, no. 4, pp. 120–122, Apr. 2001.
- [36] A. Leshem and A.-J. van der Veen, "Multichannel detection and spatial signature estimation with uncalibrated receivers," in *Proc. 11th IEEE Workshop Statist. Signal Process.*, Singapore, Dec. 2001, pp. 190–193.
- [37] A.-Z. Chen and Z.-P. Shi, "Covariance-based spectrum sensing for noncircular signal in cognitive radio networks with uncalibrated multiple antennas," *IEEE Wireless Commun. Lett.*, vol. 9, no. 5, pp. 662–665, May 2020.

- [38] F. Jalali and A. Zaimbashi, "Cognitive radio spectrum sensing under joint TX/RX I/Q imbalance and uncalibrated receiver," *IEEE Syst. J.*, vol. 14, no. 1, pp. 105–112, Mar. 2020.
- [39] A. Zaimbashi and M. S. Greco, "Multistatic passive radar target detection under uncalibrated receivers with direct-path interference," *IEEE Trans. Aerosp. Electron. Syst.*, vol. 58, no. 6, pp. 5443–5455, Dec. 2022.
- [40] A. Zaimbashi, "A unified framework for multistatic passive radar target detection under uncalibrated receivers," *IEEE Trans. Signal Process.*, vol. 69, pp. 695–708, 2021.
- [41] D. E. Hack, C. W. Rossler, and L. K. Patton, "Multichannel detection of an unknown rank- N signal using uncalibrated receivers," *IEEE Signal Process. Lett.*, vol. 21, no. 8, pp. 998–1002, Aug. 2014.
- [42] H. Urkowitz, "Energy detection of unknown deterministic signals," *Proc. IEEE*, vol. 55, no. 4, pp. 523–531, Apr. 1967.
- [43] J. Liu, H. Li, and B. Himed, "Two target detection algorithms for passive multistatic radar," *IEEE Trans. Signal Process.*, vol. 62, no. 22, pp. 5930–5939, Nov. 2014.
- [44] A. Taherpour, M. Nasiri-Kenari, and S. Gazor, "Multiple antenna spectrum sensing in cognitive radios," *IEEE Trans. Wireless Commun.*, vol. 9, no. 2, pp. 814–823, Feb. 2010.
- [45] D. Ramírez, I. Santamaría, and L. L. Scharf, *Coherence: In Signal Processing Machine Learning*. New York, NY, USA: Springer-Verlag, 2023.
- [46] P. J. Schreier and L. L. Scharf, *Statistical Signal Processing of Complex-Valued Data*. Cambridge, U.K.: Cambridge Univ. Press, 2010.
- [47] S. M. Kay, *Fundamentals of Statistical Signal Processing, Detection Theory*, vol. II. Englewood Cliffs, NJ, USA: Prentice-Hall, 1998.
- [48] R. Klemm, *Principles of Space-Time Adaptive Processing*. London, U.K.: Inst. Eng. Technol., 2006.
- [49] A. De Maio and M. S. Greco, *Modern Radar Detection Theory*. London, U.K.: Inst. Eng. Technol., 2015.
- [50] W. Liu, J. Liu, H. Li, Q. Du, and Y.-L. Wang, "Multichannel signal detection based on Wald test in subspace interference and Gaussian noise," *IEEE Trans. Aerosp. Electron. Syst.*, vol. 55, no. 3, pp. 1370–1381, Jun. 2019.
- [51] W. Liu, Y. Wang, J. Liu, W. Xie, H. Chen, and W. Gu, "Adaptive detection without training data in colocated MIMO radar," *IEEE Trans. Aerosp. Electron. Syst.*, vol. 51, no. 3, pp. 2469–2479, Jul. 2015.
- [52] E. Conte and A. De Maio, "Distributed target detection in compound-Gaussian noise with Rao and Wald tests," *IEEE Trans. Aerosp. Electron. Syst.*, vol. 39, no. 2, pp. 568–582, Apr. 2003.
- [53] P. M. Baggenstoss and S. M. Kay, "An adaptive detector for deterministic signals in noise of unknown spectra using the Rao test," *IEEE Trans. Signal Process.*, vol. 40, no. 6, pp. 1460–1468, Jun. 1992.
- [54] A. De Maio, "Rao test for adaptive detection in Gaussian interference with unknown covariance matrix," *IEEE Trans. Signal Process.*, vol. 55, no. 7, pp. 3577–3584, Jul. 2007.
- [55] W. Liu, J. Liu, L. Huang, D. Zou, and Y. Wang, "Rao tests for distributed target detection in interference and noise," *Signal Process.*, vol. 117, pp. 333–342, Dec. 2015.
- [56] M. Fazlollahpour, M. Derakhtian, and S. Khorshidi, "Rao detector for passive MIMO radar with direct-path interference," *IEEE Trans. Aerosp. Electron. Syst.*, vol. 56, no. 4, pp. 2999–3009, Aug. 2020.
- [57] A. Zaimbashi and M. Valkama, "Impropriety-based multiantenna spectrum sensing with I/Q imbalanced radios," *IEEE Trans. Veh. Technol.*, vol. 68, no. 9, pp. 8693–8706, Sep. 2019.
- [58] L. Huang, C. Qian, Y. Xiao, and Q. T. Zhang, "Performance analysis of volume-based spectrum sensing for cognitive radio," *IEEE Trans. Wireless Commun.*, vol. 14, no. 1, pp. 317–330, Jan. 2015.
- [59] A. De Maio, G. Alfano, and E. Conte, "Polarization diversity detection in compound-Gaussian clutter," *IEEE Trans. Aerosp. Electron. Syst.*, vol. 40, no. 1, pp. 114–131, Jan. 2004.
- [60] E. Conte, A. De Maio, and C. Galdi, "Statistical analysis of real clutter at different range resolutions," *IEEE Trans. Aerosp. Electron. Syst.*, vol. 40, no. 3, pp. 903–918, Jul. 2004.
- [61] E. Conte, A. De Maio, and A. Farina, "Statistical tests for higher order analysis of radar clutter: Their application to L-band measured data," *IEEE Trans. Aerosp. Electron. Syst.*, vol. 41, no. 1, pp. 205–218, Jan. 2005.
- [62] D. B. Owen, "Orthant probabilities," in *Encyclopaedia of Statistical Sciences*, vol. 6, S. Kotz and N. L. Johnson, Eds., New York, NY, USA: Wiley, 1988, pp. 521–523.
- [63] V. Bentkus, "A Lyapunov-type bound in R^d ," *Theory Probability Appl.*, vol. 49, no. 2, pp. 311–323, Jul. 2005.
- [64] K. Yosida, *Functional Analysis*, 6th ed. New York, NY, USA: Springer-Verlag, 1980.